X-ray line shapes of metals: Exact solutions of a final-state interaction model

Coenraad A. Swarts*
Department of Physics and Materials Research Laboratory, University of Illinois at Urbana-Champaign, Urbana, Illinois 61801, USA

John D. Dow
Department of Physics, Arizona State University, Tempe, Arizona 85287-1504, USA
(Received 21 July 2003; revised manuscript received 12 July 2005; published 27 October 2005)

By means of model calculations for an independent-electron metal, we obtain exact line shapes for the photon absorption, emission, and photoemission spectra of core states, including electronic relaxation. In all cases we find an x-ray edge anomaly. For the absorption and emission spectra this anomaly is superposed on a continuum resembling Elliott exciton theory. We display how the spectra evolve from the exciton limit to the free-electron limit as the final-state interaction strength is decreased or the Fermi energy increased. We compare the spectra obtained for different final-state interactions and find that different types of interactions produce different spectral shapes. Away from threshold the absorption and emission profiles show an enhancement of the free-electron result, as predicted by the screened-exciton theory. Our results offer potential explanations for (i) incompatibilities between threshold exponents and exponents extracted from other data, (ii) the occurrence of nearly symmetric x-ray photoemission lines, and (iii) the lack of mirror symmetry of absorption and emission edges.

DOI: 10.1103/PhysRevB.72.155119 PACS number(s): 78.70.Dm, 78.70.En, 68.49.Uv, 79.60.−i

I. INTRODUCTION

The explanation of the distinctive shapes exhibited at the Fermi threshold by the soft x-ray emission and absorption spectra and electron energy loss spectra of simple metals is a long-standing problem in the physics of metals, which has attracted considerable experimental[1–41] and theoretical[42–130] attention over the years.

On the basis of one-electron theory one would expect sharp Fermi-factor or step-function edges to be characteristic of simple free-electron metals,[42] in disagreement with the observed spectra. For instance, the $L_{\mathrm{II,III}}$ edges of Na,[1–11] Mg,[1,4,6,7,10–20] and Al,[1,4,6,7,11,12,14–17,19,21–23] as well as the $M_{\mathrm{II,III}}$ edge of K,[24–26] are sharp but slightly peaked while the K edges of Li,[1,3,6,7,13,14,19,20,23,27–35] Mg,[10–20] and Al (Refs. 11–23) are broad and rounded. Transitions from the outermost p shells of Rb and Cs yield line shapes similar to the $L_{\mathrm{II,III}}$ edge shapes of Na, Mg, and Al,[25,26] but the spectra of rare-gas impurities in alkali-metal hosts mysteriously exhibit ramp thresholds,[39] and the soft x-ray lineshapes of binary alloys[13–15,20,25,26,37] such as $\mathrm{Li}_{1-x}\mathrm{Mg}_x$ sometimes have threshold behaviors quite different from the edge shapes of their metallic components. Gupta *et al.*[80–82] have shown that by taking band-structure effects into account in the one-electron theory, one obtains spectra with the qualitative features observed in the spectra of Na and Mg. Thus band-structure effects may be important for understanding edge shapes, even in free-electron metals. However, the question remains whether one-electron theory alone can quantitatively account for the observed spectra. The one-electron method does not take into account the final-state interaction or the electronic relaxation, effects believed to cause divergent enhancements of absorption and emission spectra at the Fermi threshold.

A simple approach that seeks to remedy some of the deficiencies of one-electron theory is the so-called screened-exciton approximation.[62] This method takes into account some of the effects of the final-state interaction by replacing the unperturbed conduction band states by new states, perturbed from the old ones by the screened potential associated with the core hole. In certain limits (see Sec. IV B), this approximation describes the gross features of spectra very well, especially for energies far from the Fermi threshold; however, no peaks at threshold are predicted within the screened-exciton approximation, because the only electronic relaxation accounted for is the distortion of the optical electron's orbit by the core hole. The relaxation of the electrons in the Fermi sea is omitted, and it is this effect that is thought to produce the singular threshold.

Friedel[43,44,48] first suggested that electron-hole interactions and multi-electron relaxation are responsible for interesting modifications of the one-electron line shapes in metals. This was subsequently expanded upon by Mahan,[45] Mizuno and Ishikawa,[46] and Nozières and de Dominicis (ND),[47] who developed an asymptotic theory for the threshold behavior of the absorption and emission spectra of free-electron metals. The ND theory is based on the fact that the sudden insertion of a core hole into a metal during x-ray absorption is equivalent to the sudden application of a potential to the conduction electrons, and causes the conduction sea to recoil into a distribution of excited-state configurations. Nozières and de Dominicis simulate this by describing the conduction electron sea with different Hamiltonians for the initial and final states; they use an initial Hamiltonian H_{initial} for N conduction electrons in a potential $U(r)$:

$$H_{\mathrm{initial}} = \sum_{j=1}^{N} [(p_j^2/2M) + U(r_j)]. \tag{1.1}$$

This is then suddenly switched to a final Hamiltonian

$$H_{\text{final}} = \sum_{j=1}^{N} [(p_j^2/2m) + U(r_j) + V(r_j)], \quad (1.2)$$

which differs from the initial Hamiltonian by the final-state interaction $V(r)$. We have $M=N$ for x-ray photoemission spectroscopy (XPS),[131–136] and $M=N+1$ $(N-1)$ for x-ray absorption (emission). With this model, ND obtain an asymptotic solution for the absorption lineshape $\kappa(E)$ for $N \rightarrow \infty$ and $E \rightarrow E_T \equiv E(T)$, which shows an edge anomaly given by

$$\kappa(E) = A(E - E_T)^{-1+\gamma}\Theta(E - E_T). \quad (1.3)$$

Here E_T is the threshold energy, A is a constant, Θ is the unit step function, and γ is an exponent related to the difference of the phase shifts of the perturbed and unperturbed one-electron states at the Fermi energy (see Sec. II B). The asymptotic line shape for emission is the mirror image of Eq. (1.3) about the threshold energy. A similar expression, with a slightly different exponent, was obtained for the XPS lineshapes by Doniach and Sunjic.[52]

The ND model has experienced several different levels of acceptance. Initially it was combined with predictions of exponents[45,51] and thought to provide the explanation of the rounded K edges. Indeed the explanation of the K edge rounding as an electronic relaxation effect was thought to be the greatest triumph of the theory.[65] However, subsequent work[30–35,41,55] demonstrated that the K edge rounding originates from phonon[36,50,54,72,134] and Auger[59] effects and not from the Fermi threshold effect. There now exists consensus on the origin of the K edge broadening, although some discussion continues concerning the sizes of the various contributions.[109] The failure of the theory in its original form for the K edges stemmed primarily from the exponent predictions, which were based on the excessively large phase shifts of Thomas-Fermi screened potentials[110] and not on the ND model itself.

Attention then focused on claims that the ND relaxation is the cause of the peaked $L_{\text{II,III}}$ and $M_{\text{II,III}}$ edges. Unlike the discussion of the rounded K edges, which centered on *qualitative* aspects of the theory, the peaked edge debate concentrated on *quantitative* line shape analyses. The ND line shape Eq. (1.3) was first fitted to the $Mg_{1-x}Sb_x$ absorption edge data of Slowik and Brown,[38,58] producing values of the absorption edge exponent γ (also called α_0).[137] Subsequent analyses of the $L_{\text{II,III}}$ absorption and emission edges of Na, Mg, and Al also yielded values of α_0.[57] A controversy swirled around these analyses for a while, with several workers doubting that accurate exponents could be extracted from the data; however, analyses of subsequent experiments[35] have generally confirmed the early exponents while reducing the experimental uncertainties. The exponents extracted from fitting edge data with suitably broadened forms of Eq. (1.3) are not necessarily the "true" exponents, however, and contemporary work focuses on the corrections to the asymptotic theory Eq. (1.3) due to band structure, exchange, and electron-electron interactions—because widespread inconsistencies have been found among exponents extracted from $L_{\text{II,III}}$ edges,[56] XPS data,[88] electron-energy-loss spectra,[83] impurity resistivity data,[74] and impurity absorption data.[39] Although resolutions of a small number of these discrepancies have been proposed,[85,135] no consistent theory of all the data has been set forth; the most serious inconsistencies involve the XPS exponents[88] and remain unexplained today. Thus workers in the field now seem to agree that the ND threshold effect is not the *sole* cause of the observed edge anomalies, but no consensus has been reached on the quantitative importance of the various other physical phenomena contributing to the edge shapes.

On the theoretical side, there has been general unanimity that Eq. (1.3) is the correct asymptotic solution to the ND model *at threshold*. The extent to which it remains faithful to the exact solutions away from threshold is a topic of ongoing discussion.

Four possibilities are often mentioned as possible causes of the discrepancies between the asymptotic ND theory and data: (i) one-electron band-structure effects possibly produce an energy dependence in the "constant" A of Eq. (1.3);[80–82,88] (ii) exchange mixing of spin-orbit split edges is perhaps significant;[76,95] (iii) many-electron effects omitted from the ND model conceivably distort the edge shapes;[84,103] and (iv) exact solutions of the ND model perhaps disagree with the asymptotic solution Eq. (1.3), for energies a significant distance from threshold.

This last possibility motivates the present work. The asymptotic solution is reminiscent of critical behavior in phase transition theory: a universal asymptotic threshold behavior Eq. (1.3) exists for all final-state interactions yielding the same change of Fermi energy phase shift. But in phase transitions, the universal behavior is often only apparent very near the critical temperature: $|(T-T_c)/T_c| \ll 10^{-2}$. If, by analogy, the asymptotic theory were comparably limited to energies very near threshold, then the asymptotic regime would not be accessible to contemporary experiments, which are limited by instrumental or lifetime broadenings to resolutions of greater than 0.05 eV.

The ND model for free-electron metals can be solved exactly for the XPS, absorption, and emission profiles, even for realistic final-state interactions, as demonstrated by Dow and Flynn[90] and by Flynn and the authors,[96] using determinants and a finite number of electrons in the Fermi sea. Other authors,[61,86,87,91,92,97] most notably Kotani and Toyozawa[61] and Grebbenikov *et al.*,[92] have provided solutions of various versions of the ND model using the Green's function method; the most extensive theoretical solutions involve model densities of states and separable final-state interactions. (Computationally the determinantal method presented here appears to be faster as well as better suited to the treatment of realistic systems.) Extensions of the determinantal method to p-wave recoil,[99] "forbidden" transitions,[100] and a model of rare-gas impurities in alkali-metal hosts[113] have likewise been published. The method has also been used to study Auger spectra[112] and the effects of band structure,[138] surfaces,[139] high temperatures,[140] and disorder[141] on x-ray edges. For the models treated, the asymptotic theory Eq. (1.3) and the exact solutions agree at threshold,[142] but significant differences occur between the exact and asymptotic solutions at energies away from threshold, with the size of the differences depending on the final-state interactions. This

raises the possibility that the XPS exponents, which are obtained by fitting data over the most extended energy range, may be the least accurate approximation to the "true" exponents—so that some of the most serious discrepancies between the asymptotic theory and data may be resolved.[90]

In this paper we shall present a complete discussion of how the ND model can be solved exactly to obtain profiles for XPS, absorption, and emission. Sum rules can be employed to check the results of these calculations and screened-exciton theory[62] can be used to predict the asymptotic high-energy absorption profile and the gross features of the spectra. Furthermore, it will be shown that the exact solutions correctly describe the formation of a second threshold in the XPS and absorption spectra if the final-state interaction is strong enough to produce a bound state. The XPS spectra also display resonances. In each case we find that the exact solution and the ND result agree only very close to threshold, showing that the ND theory is a true asymptotic theory. However, for energies at finite distances from threshold, differences between the exact and asymptotic line shapes appear. Hence we urge caution in the interpretation of experimental exponents extracted from line shapes by fitting the asymptotic theory over an extended energy range: our calculations suggest that the experimental exponents may not be the "true" exponents.

We have restricted ourselves to calculations of the line shape for *s*-wave channels alone. This serves to illustrate the features of the exact solutions, although the methods are not restricted to this case and have been applied successfully to other channels as well.[99–101] Furthermore, for mathematical convenience, we have considered only final-state interactions $V(r)$ for which overlap integrals of initial- and final-state single-particle wave functions can be evaluated analytically once the wave functions are known.

The organization of this paper is as follows. In Sec. II we describe how exact solutions for the XPS recoil profiles may be obtained for systems containing a finite number of electrons N. It is also shown how the solution for $N\rightarrow\infty$ can be obtained from these exact solutions for finite N. In Sec. III we give the results of our calculations of the XPS recoil profiles for four different final-state interactions, and compare these results with profiles obtained using the ND theory. Section IV describes how exact solutions of the absorption and emission profiles are obtained for systems with a finite number of electrons; this section also contains a description of screened-exciton theory and its applications to various final-state interactions. In Sec. V we give the results for the emission and absorption spectra, and compare the exact results with profiles obtained with other theories. Section VI contains a discussion of our results. Finally, in the Appendix, we give some of the mathematical details of the calculations. Throughout this paper we use units such that $(h/2\pi)^2=2m$, $e^2=2$; i.e., the Rydberg Ry is the unit of energy and the Bohr radius a_B is the unit of length.

II. EXACT SOLUTIONS FOR XPS

A. Solutions for a finite number of electrons

Following ND[47] and Dow and Flynn[90] we consider a noninteracting Fermi sea of conduction electrons described by the initial and final Hamiltonians given in Eqs. (1.1) and (1.2). In the case of x-ray photoemission spectroscopy, the core electron is removed to infinity, the number of conduction electrons does not change ($M=N$), and we are interested in the recoil profile $I(E)$ given by

$$I(E)=\sum_{f\nu}|\langle i|f\nu\rangle|^2\delta(E-E_{f\nu}+E_i). \tag{2.1}$$

Here $|i\rangle$ and $|f\nu\rangle$ are the N-electron initial and final states (Slater determinants) of the conduction electrons and

$$\langle i|f\nu\rangle=\det(\phi_n,\psi_m), \tag{2.2}$$

where $|\phi_n)$ and $|\psi_m)$ are one-electron initial and final states, respectively. When the conduction Fermi sea is noninteracting and contains only a few electrons, the recoil profile $I(E)$ can be evaluated exactly for any final-state interaction $V(r)$. In particular, for a spherically symmetric system with isotropic potentials $U(r)$ and $V(r)$ at its center, the total recoil profile is a multiple convolution of profiles $I_{\ell ms}(E_{\ell m\sigma})$ for each individual angular momentum channel $\ell m\sigma$:[90]

$$I(E)dE=\prod_{(\ell,m,\sigma)=(0,-\ell,-1/2)}^{(\infty,\ell,1/2)}I_{\ell m\sigma}dE_{\ell m\sigma}. \tag{2.3}$$

Here $E_{\ell m\sigma}$ is the recoil energy in the $\ell m\sigma$ channel and we have $E=\Sigma_{\ell m\sigma}E_{\ell m\sigma}$. This shows that we need only consider one channel at a time and in what follows we consider only a single-spin *s*-wave channel.

To calculate the *s*-wave recoil profile for N *s*-electrons we go through the following steps: (i) specify the potential $U(r)$ present in the initial state; (ii) specify the electron density n (using $n^{-1}=4\pi r_s^3/3$), and hence the Fermi wave vector k_F and the Fermi energy E_F; (iii) enclose the system in a box of radius R determined by the number of electrons N and the Fermi wave vector k_F; (iv) solve the Schrödinger equation for the initial single-particle orbitals $|\phi_n)$; (v) specify δ_0, the difference in phase shifts at the Fermi level for the perturbed and unperturbed single-particle states: (vi) adjust the parameters of the final-state interaction $V(r)$ to produce this phase shift difference δ_0; (vii) solve the Schrödinger equation for the perturbed single-particle states $|\psi_m)$; (viii) enumerate all possible final-state configurations $|f\nu\rangle$ and form the appropriate determinants $\langle i|f\nu\rangle=\det(\phi_n,\psi_m)$; (ix) evaluate the profile $I(E)$ using Eqs. (2.1) and (2.2).

To make these steps clearer, we shall consider, as an example, the simple case first discussed by Dow and Flynn[90] of suddenly impressing an infinite barrier potential on an electron gas. Here we choose $U(r)=0$ in Eqs. (1.1) and (1.2), and specify the electron density by r_s. Then we have $k_F(9\pi/4)^{1/3}/(r_s a_B)$ and $R=N\pi/k_F$. The initial single-particle orbitals are given by

$$|\phi_n)=(2\pi Rr^2)^{-1/2}\sin(k_n r), \tag{2.4}$$

with $k_n=n\pi/R$ and $n=1,2,\ldots,N$. Let the phase shift at the Fermi level be δ_0 and choose $V(r)=\infty$ for $r<a$ and $V(r)=0$ for $a<r<R$ (i.e., an infinite barrier of radius a at the center of the system). Then we must have $a=\delta_0/N\pi$ to produce the

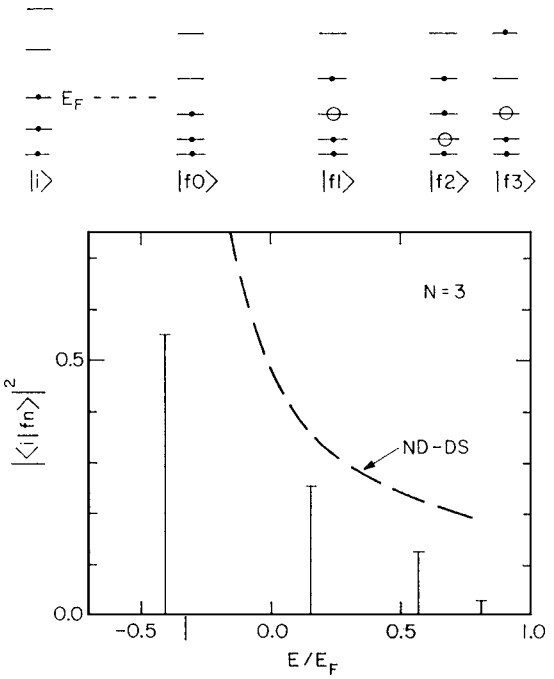

FIG. 1. Single-particle energy levels and their occupancies in the initial state $|i\rangle$ and various final states $|f\nu\rangle$ for $N=3$. The lower portion of the figure gives the numerical recoil profile for this case, as well as the ND-DS (Nozières–de Dominicis or Doniach-Sunjic) profile (dashed).

desired phase shift. The final-state single-particle orbitals for this case are given by

$$|\psi_m) = [2\pi(R-a)r^2]^{-1/2} \sin[k'_m(r-a)], \qquad (2.5)$$

for $a<r<R$, with $k'_m=m\pi/(R-a)$ and with m taking on all integer values. To illustrate the enumeration of the possible final-state configurations let us consider a system of $N=3$ s waves, and denote the configurations by $|n_1,n_2,n_3\rangle$, where the n_i denote the occupied single-particle orbitals of the final-state configuration. Various possible final-state configurations of orbitals $|\psi_m)$ are the ground state $|f0\rangle=|1,2,3\rangle$ and states with one electron-hole pair such as $|f1\rangle=|1,2,4\rangle$, $|f2\rangle=|1,3,4\rangle$, and $|f3\rangle=|1,2,5\rangle$. Also possible, of course, are states with multiple electron-hole pairs, such as the two-pair state $|1,4,5\rangle$. The initial state is a Slater determinant of the three lowest orbitals $|\phi_1)$, $|\phi_2)$, $|\phi_3)$. It is now a simple matter to evaluate the various contributions $|\langle i|f\nu\rangle|^2 = \det^2(\phi_n,\psi_m)$ to the recoil profile, as well as the energies at which these contributions occur, and thereby evaluate the complete recoil profile for $N=3$. An example is given in Fig. 1, where we show the initial state $|i\rangle$ as well as various final-state configurations $|f0\rangle$, $|f1\rangle$, $|f2\rangle$, and $|f3\rangle$. (This example in Fig. 1 corresponds to an attractive final-state interaction rather than a repulsive one.) Also shown are the zero-pair line $|\langle i|f0\rangle|^2$ and some single-pair lines $|\langle i|f\nu\rangle|^2$.

The total number of final-state configurations is of course infinite, but fortunately it turns out that only a few excitations close to the ground state are needed to obtain the complete recoil profile. To demonstrate this, it is convenient to consider the integrated recoil profile $J(E)$ given by

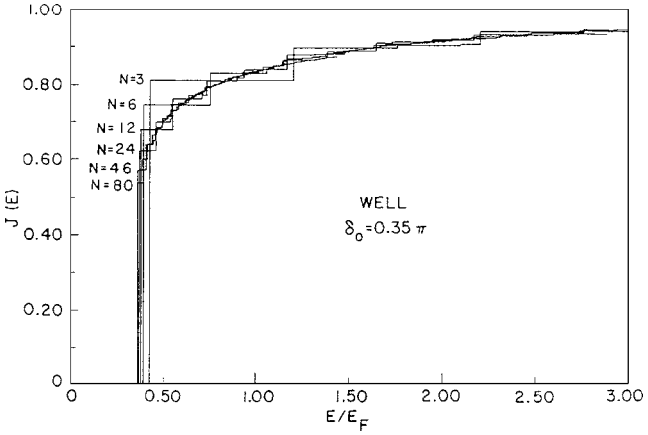

FIG. 2. Typical integrated recoil spectrum $J(E)$ versus energy in units of the Fermi energy, for $N=3$, 6, 12, 24, 46, and 80. These spectra for a square well with phase shift $\delta_0=0.35\pi$ illustrate how rapidly the calculations for finite N approach the infinite-N limit.

$$J(E) = \int_{E(T)}^{E} I(E')dE' = \sum_{f\nu} |\langle i|f\nu\rangle|^2 \Theta(E-E'), \qquad (2.6)$$

where $E(T)$ is the same as E_T. This integrated profile obeys the sum rule

$$J(\infty) = \sum_{f\nu} |\langle i|f\nu\rangle|^2 = 1. \qquad (2.7)$$

Since $J(\infty)=1$ we know that the calculation has converged as soon as $J(E)$ differs from unity by a sufficiently small number; once this condition is satisfactorily met, it is no longer necessary to consider additional highly excited states. From the integrated recoil profiles shown in Fig. 2 for $N=3$, 6, 12, 24, 46, and 80, it is clear that the calculation has saturated the sum rule (2.7) for excitation energies of the order of $2E_F$, i.e., for a finite number of excitations. Moreover, it turns out that only excitations consisting of one or two electron-hole pairs are important (unless the final-state interaction produces one or more bound states, in which case excitations consisting of three or more electron-hole pairs may become important; in those cases, however, the single-pair excitations often become unimportant). From Fig. 2 it is also clear that the profile has an essential stability which manifests itself for $N\approx 10$; larger systems merely smooth the response obtained for $N\approx 5$. Figure 2 also shows that the procedure has converged to the large-N result for $N=80$. In the next subsection we shall discuss how one may obtain the exact line shape for $N\to\infty$ from these numerical results for finite N.

B. Limit of infinite number of electrons

The strength of the zero-pair line $|\langle i|f0\rangle|^2$ can be obtained from Anderson's[143] orthogonality theorem, which states that

$$|\langle i|f0\rangle|^2 = CN^{-\Xi}, \quad \text{where } \Xi = (\delta_0/\pi)^2, \qquad (2.8)$$

where C is a constant slightly less than unity. [For large N, our calculated values of $\langle i|f0\rangle$ scale as required by Eq.

(2.8).] From this, one can simply obtain the ND result, as first shown by Flynn,[90] as follows: the strength of the zero-pair line is the integral of the line shape from threshold $E(T)\equiv E_T$ to the first pair line, which occurs at energy $E=E_T+2E_F/N$:

$$|\langle i|f0\rangle|^2 = \int_{E(T)}^{E_T+2E_F/N} I(E')dE' = CN^{-\eta}, \quad \text{where } \eta=(\delta_0/\pi)^2. \tag{2.9}$$

If the lineshape becomes sufficiently independent of N for large N,[108] we obtain by differentiation with respect to N and substitution of $E=E_T+2E_F/N$:

$$I(E) = A(E-E_T)^{-1+\Delta_0}\Theta(E-E_T), \tag{2.10}$$

for $E\to E_T$, where $\Delta_0=(\delta_0/\pi)^2$ and $A\approx C\Delta_0(2E_F)^{-\Delta_0}$.[108] Equation (2.10) is simply the one-channel ND result, as obtained for photoemission by Doniach and Sunjic.[52] For the integrated profile one obtains

$$\begin{aligned} J(E) &\approx (A/\Delta_0)(E-E_T)^{\Delta_0}\Theta(E-E_T) \\ &= C[(E-E_T)/2E_F]^{\Delta_0}\Theta(E-E_T). \end{aligned} \tag{2.11}$$

The constant A, which is related to Anderson's constant C,[108] can be obtained from the numerical results by calculating C as a function of $1/N$ from Eq. (2.8) and extrapolating the results to $1/N=0$. The threshold energy E_T can be obtained analytically for some final-state interactions, while for other cases it can be calculated numerically for some large value of N (typically $N=5000$). We now fit our numerical results with a line shape

$$J(x) = C(x/2)^{\Delta(x)} \quad \text{for } x<2, \tag{2.12}$$

where we have $x=(E-E_T)/E_F$, and $\Delta(x)=\Delta_0+\Sigma_{p=1}^{5}b_p x^p$. This procedure works only for $x<2$. Since we know that $J(x)$ approaches unity for large x, we also use

$$J(x) = 1-\exp\left(\sum_{p=0}^{4} c_p x^p\right) \quad \text{for } x>1. \tag{2.13}$$

By taking derivatives of Eqs. (2.12) and (2.13), we are in general able to obtain an accurate line shape $I(E)$. As a check on the fit and to remove any ambiguities in the fitted line shapes, especially in the region $1<x<2$, where the two fits overlap, we have also convolved the numerical line shapes $I(E_n)$ with a Gaussian of width Γ comparable to the level spacing, $\Gamma=2E_F/N$, to obtain a broadened recoil profile I_G:

$$I_G(E) = \sum_{n=1}^{N'} (2\pi\Gamma^2)^{-1/2}\exp[-(E-x_n)^2/2\Gamma^2]I(x_n). \tag{2.14}$$

Here N' stands for the number of calculated points of the numerical line shape and $I(x_n)$ is the calculated intensity at $E=x_n$.

Finally we notice that the exact calculations also provide us with the recoil energy E_R for a particular channel, defined as

$$E_R = E_{f0}-E_i = \sum_{m=1}^{M}\epsilon_m^f - \sum_{n=1}^{N}\epsilon_n^i, \tag{2.15}$$

where ϵ_m^f and ϵ_m^i are the energies of the one-electron orbitals in the final and initial states, respectively. The recoil energy E_R can be evaluated exactly in some cases, while in cases where this is not possible E_R can be evaluated numerically for some large value of N (typically $N=5000$).

III. RESULTS FOR XPS RECOIL PROFILES

We have considered four forms of the final-state interaction $V(r)$, namely, (i) a repulsive barrier, (ii) an attractive square well, (iii) an attractive δ shell, and (iv) a repulsive δ shell. In this section we shall give the results for each of those cases separately in Secs. III A–III D. All calculations have employed an electron density appropriate for Na ($r_s=3.93$). Some mathematical details of the calculations are given in the Appendix.

A. Repulsive barrier

In the first place we have considered a repulsive barrier $V_B(r)$ of infinite strength

$$V_B(r) = \begin{cases} \infty & \text{for } r<a, \\ 0 & \text{for } r>a. \end{cases} \tag{3.1}$$

The radius a is determined by the phase shift difference δ_0 at the Fermi level, as described in Sec. II A. We consider two cases, namely, (i) $\delta_0>0$, in which case we take $U(r)=V_B(r)$, $V(r)=-V_B(r)$ in Eqs. (1.1) and (1.2); and (ii) $\delta_0<0$, in which case we choose $U(r)=0$, $V(r)=V_B(r)$. Case (i) corresponds to "turning the barrier off" in the final state. The case of the infinite barrier was selected mainly for its simplicity, although it may be of some relevance in the ionization of an electron bound to a neutral rare-gas impurity in a metal [case (i)],[39] as well as in the capture of negative mesons in metals [case (ii)].[144]

For the infinite barrier the recoil energy E_R (and also the threshold energy E_T) can be evaluated exactly in the limit $N\to\infty$, and is given by

$$E_R = (2\delta_0/3\pi)E_F. \tag{3.2}$$

In Fig. 3 we show our results for the recoil profile $I(E)$ for various phase shifts δ_0. Also shown are the ND profiles normalized with Anderson's constant as discussed above. The profiles for positive phase shifts are displayed to the right of the threshold (which is arbitrarily set equal to zero), while those for negative phase shifts are displayed to the left of threshold.

For small phase shifts ($|\delta_0|<0.125\pi$) the XPS sum rule [Eq. (2.7)] is adequately exhausted very close to threshold and the exact calculations and the ND results appear at first glance to agree well. However, percentagewise the difference between the exact calculations and the ND profiles is $\approx 20\%$ for $(E-E_T)/E_F=0.1$. It is also clear that the profiles are not symmetric under a change in sign of δ_0, except infinitesimally close to threshold. For larger phase shifts this mirror

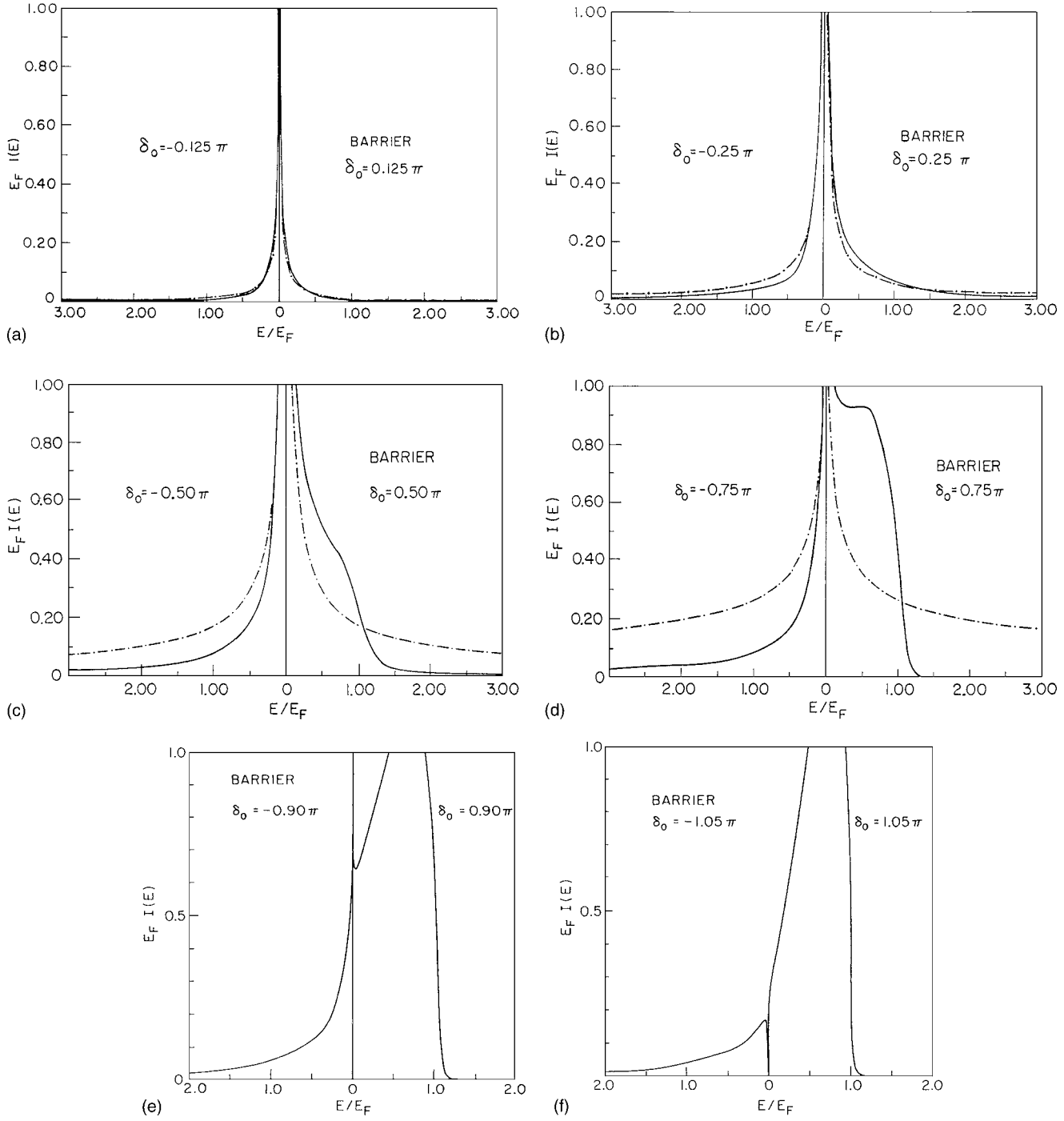

FIG. 3. Recoil profiles $E_F I(E)$ for barriers of infinite height, with phase shifts $|\delta_0|=0.125\pi$, 0.25π, 0.50π, 0.75π, 0.90π, and 1.05π. Profiles for positive phase shifts are displayed to the right of the threshold (turning off the barrier), those for negative phase shifts are displayed to the left of the threshold (turning on the barrier). Solid lines, exact results; chained lines, ND theory.

asymmetry becomes more pronounced, as in general the profile for $\delta_0>0$ shuts off for $E\approx E_F$, while the profile for $\delta_0<0$ does not display this behavior. This asymmetry is observed for all final-state interactions considered in this work, and points to a basic asymmetry in the recoil profiles for cases with $\delta_0>0$ and $\delta_0<0$, respectively. For $\delta_0>0$ the final-state interaction is attractive and causes the one-electron orbitals of the final state to have lower energies than the corresponding orbitals of the initial state. This means that the initial state can be expanded approximately in those final states made up out of single-particle states with energies $\leqslant E_F$ (i.e., the first $N+1$ single-particle final states). Note that the maximum excitation energy for these excitations is $\approx E_F$, corresponding to an excitation from the $n=1$ level to the $n=N+1$ level. (If a bound state is present, we should add ϵ_B, the binding energy of the bound state. See also Flynn[84] for a discussion along these lines for a very simple case.) Therefore, on the one hand for $\delta_0>0$, one expects the profile to

show a cutoff at excitation energies near E_F. The effect becomes more pronounced for large phase shifts δ_0. On the other hand, for $\delta_0<0$ one cannot expect the profile to show such a cutoff at excitation energies near E_F. This is because the final-state interaction is now repulsive, causing the one-electron orbitals of the final state to have higher energies than the corresponding orbitals in the initial state. Therefore, it is no longer possible to expand the initial state approximately in final states made up out of single-particle states with energies below E_F, and no cutoff at excitation energies near E_F is expected. (In this case it would be possible to expand the final ground state approximately in a number of initial states with single-particle energies below E_F, thus re-establishing the symmetry between the two cases. However, this is a moot point, since one has to consider only the initial ground state.) In principle it is possible to confirm these observations with the moment theorems derived by Flynn[39,72,84].

From these results it is already clear that the ND theory is valid only very close to threshold (the exact result and the ND results start to differ substantially for $E-E_T\approx 0.03E_F$), and that the use of the ND theory to fit experimental line shapes away from threshold may introduce significant errors.

The exhaustion of the XPS sum rule [Eq. (2.7)] at energies near threshold suggests an explanation of the anomalously symmetric XPS lines:[88] the asymmetry at threshold is obscured far from the threshold by instrumental broadening, because the sum rule prevents the line shape from having a prominent tail at energies far from threshold.

As the phase shift approaches π, the divergence at the threshold becomes less pronounced as $(\delta_0/\pi)^2$ approaches unity, until finally for $|\delta_0/\pi|>1$, the divergence disappears and the profiles become broad and rounded, as shown in Fig. 3 for $|\delta_0/\pi|=1.05$.

Finally we notice that, for the barrier, the spectra $E_F I(E)$ plotted against $(E-E_T)/E_F$ depend only on δ_0, not on r_S. Thus the spectra displayed in Fig. 3 are in fact valid for all r_S, when appropriately scaled.

B. Attractive square well

It may be argued that the previous case of the infinite barrier is not a good case to consider, since the eigenstates for the problem with the barrier present do not form a complete set of states for the case where the barrier is absent, so that Eq. (2.7) does not necessarily hold [although numerically we find that Eq. (2.7) is satisfied in a limiting sense for large but finite barriers.[113]] For an attractive square well this problem does not occur. Here we use the square well potential $V_W(r)$ given by

$$V_W(r) = V_0\Theta(a-r). \tag{3.3}$$

We arbitrarily choose $a=1.5a_B$, after which the strength $|V_0|$ of the potential is determined by δ_0, the phase shift at the Fermi level. For $\delta_0>0$ we choose $U(r)=0$ and $V(r)=V_W(r)$ in Eqs. (1.1) and (1.2), while for $\delta_0<0$ we have $U(r)=V_W(r)$ and $V(r)=-V_W(r)$. In other words, a positive phase shift corresponds to turning the square well potential on, while a negative phase shift corresponds to turning the potential off. In this case the recoil energy cannot be evaluated exactly and was instead determined numerically for $N=5000$. The recoil energies so obtained for various phase shifts are given in Table I. In Fig. 4 we show the results of our calculations for $I(E)$ for various values of δ_0, together with normalized ND profiles. These spectra depend on a/r_S (for given δ_0), and a/r_S was chosen to be $0.38a_B$, i.e., a well radius of $1.5a_B$ for an electron gas of $r_S=3.93$.

TABLE I. Recoil energies E_R/E_F for XPS profiles for the square well and the attractive and repulsive δ shells. All recoil energies are calculated for $N=5000$ and $r_S=3.93$. Values given are for positive phase shifts; for negative phase shifts all the signs change.

	E_R/E_F	
δ_0/π	First threshold	Second threshold
	Square well	
0.050	−0.0354	
0.100	−0.0738	
0.125	−0.0945	
0.250	−0.2170	
0.350	−0.3581	
0.450	−0.5828	0.4632
0.750	−6.5440	0.1690
	Attractive δ shell	
0.050	−0.0334	
0.100	−0.0688	
0.250	−0.1953	
0.500	−0.6373	0.4224
0.750	−2.0980	0.1784
	Repulsive δ shell	
0.100	−0.0429	
0.125	−0.0839	
0.250	−0.1685	
0.350	−0.2363	
0.500	−0.3416	
0.750	−0.5015	

The spectra displayed in Fig. 4 show the same qualitative features as the spectra obtained for the repulsive barrier: for small phase shifts the sum rule is exhausted very close to threshold, whereas for larger phase shifts the profiles for $\delta_0>0$ shut off near $E-E_T=E_F$, while those for $\delta_0<0$ do not. A new feature in this case is the appearance of a second threshold for $\delta_0>0.38\pi$, i.e., when the potential is strong enough to form a bound state. This second threshold corresponds to a final state differing from the ground final state $|f0\rangle$ by the excitation of an electron in the bound state to the first empty orbital above the Fermi level, and this second threshold occurs at an energy $E_F+\epsilon_B$ above the first threshold, where ϵ_B is the binding energy of the bound state. A similar second threshold was obtained by Davis and Feldkamp.[97] A second threshold is not present for $\delta_0<-0.38\pi$, since in that case the attractive potential is present in the initial state, which is always assumed to be the ground state, so that the bound state is always occupied. At finite temperatures, however,

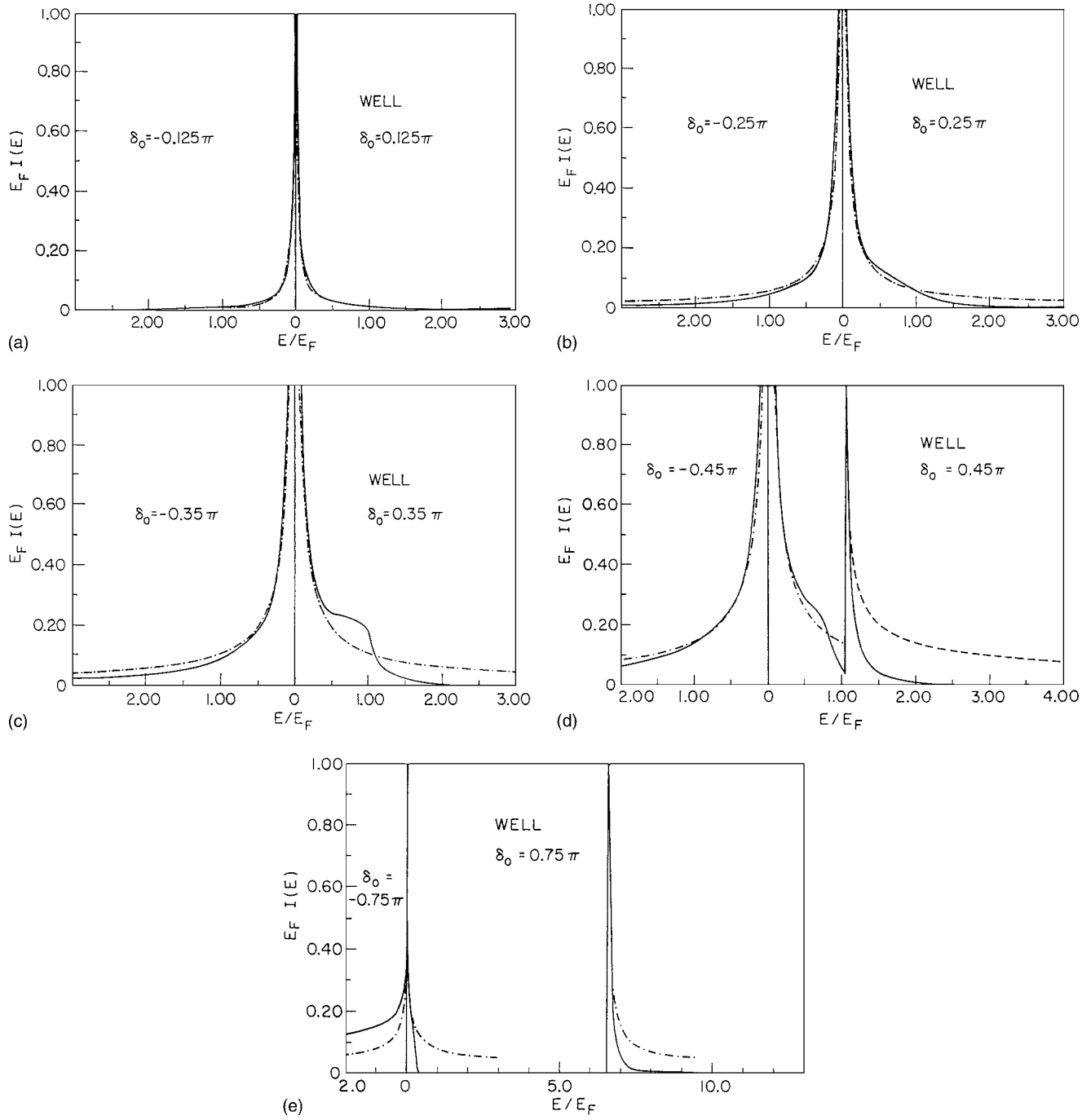

FIG. 4. Recoil profiles $E_F I(E)$ for turning on a square well of radius $a=1.5a_B$ ($a/r_s=0.38a_B$); as in Fig. 3. The phase shifts are $|\delta_0|=0.125\pi$, 0.25π, 0.35π, 0.45π, and 0.75π. The profiles for turning off the wells are given on the left.

such a second threshold would appear; such a situation can occur in doped semiconductors with $E_F \approx k_B T$.[140]

To obtain the profile at the second threshold E_Y as $N \to \infty$, we again use Anderson's theorem, Eq. (2.8), but now with an exponent equal to $(\delta_0/\pi - 1)^2$, i.e.,

$$|\langle i|f0'\rangle|^2 = CN^{\xi}, \quad \text{where } \xi = (\delta_0/\pi - 1)^2, \tag{3.4}$$

where $|f0'\rangle$ denotes the lowest-energy final state in which the bound orbital is unoccupied. This expression follows since the excess localized charge in the s-wave channel is $(\delta_0/\pi) - 1$ in this case, in contrast with δ_0/π for the true ground state $|f0\rangle$.[49,53] In the same way as Eq. (2.10) was obtained from Eq. (2.8) we now obtain from Eq. (3.4)

$$I(E) = A_2(E - E_{T2})^{-1+\Delta}\Theta(E - E_{T2}), \tag{3.5}$$

or

$$J(E) = C_2[(E - E_{T2})/2E_F]^{\Delta}\Theta(E - E_{T2}), \tag{3.6}$$

where A_2 and C_2 are constants and we have $\Delta = (\delta_0/\pi - 1)^2$. The lineshape for $N \to \infty$ is now obtained from the line

shapes for finite N in the same way as described in Sec. II B for the first threshold.

As a check on the calculation we can still employ the sum rule Eq. (2.7) for the total integrated spectrum. It would be convenient, however, to be able to separate this integrated profile into a contribution from final states in which the bound state is occupied, and a contribution from final states in which the bound orbital is empty. It is possible to obtain an approximate expression for the contribution $J_B(\infty)$ from final states in which the bound state is occupied. We have

$$J_B(\infty) = \sum_{f\nu(B)} |\langle i|f\nu_B\rangle|^2 = \sum_{j<\ell<\cdots<n} \begin{vmatrix} (\phi_1|\psi_B) & (\phi_1|\psi_j) & (\phi_1|\psi_\ell) & \cdots & (\phi_1|\psi_n) \\ (\phi_2|\psi_B) & (\phi_2|\psi_j) & (\phi_2|\psi_\ell) & \cdots & (\phi_2|\psi_n) \\ \cdots & & & & \\ \cdots & & & & \\ \cdots & & & & \\ \cdots & & & & \\ (\phi_N|\psi_B) & (\phi_N|\psi_j) & (\phi_N|\psi_\ell) & \cdots & (\phi_N|\psi_n) \end{vmatrix}^2 . \tag{3.7}$$

Here the occupied final orbitals are $|\psi_B\rangle, |\psi_j\rangle, |\psi_\ell\rangle, \ldots, |\psi_n\rangle$. We expand the determinant with respect to the first column and note that the minors $M_{q,1}$ of the first column represent overlaps of two $(N-1)$-electron states, the initial state made up out of all initial one-electron orbitals except $|\phi_q\rangle$, and the final state made up out of all the same one-electron continuum states as the original determinant. Assuming that the initial states can be expanded in a complete set of final continuum states, we can carry out the sum and obtain

$$J_B(\infty) \approx \sum_{j=1}^{N} |(\phi_j|\psi_B)|^2. \tag{3.8}$$

This expression is only approximate, since we do not sum over a complete set of final states; the bound state is missing. However, the numerical calculations indicate that Eq. (3.8) is very closely satisfied in all the cases we have considered, and so this equation does provide us with a useful check on the numerical calculations.

As the potential becomes stronger, leading to a deep bound state, the divergence at the second threshold $E_{T2} \equiv E(T2)$ also becomes stronger, while the divergence at the first threshold becomes weaker. This means that simultaneous excitations of two electrons (one of which is excited out of the bound orbital) become more important than they were in the case of no bound state. Similarly, for sufficiently strong potentials, two or more bound states may be formed (not shown in the figures), in which case excitations involving three or more electrons may become important.

At the second threshold we see once again that the ND result and the exact calculations agree only very close to the threshold.

C. Attractive δ shell

Another form of the final-state interaction for which the overlap integrals can be evaluated analytically is a δ shell of radius a:

$$V_{\delta-}(r) = -V_0 a\,\delta(r-a). \tag{3.9}$$

Here we choose $V_0 a = 1.5 a_B$ Ry for $|\delta_0/\pi| \leq 0.5$, and $V_0 a = 6.0 a_B$ Ry for $|\delta_0/\pi| = 0.75$. With these choices for $V_0 a$, the radius a is determined by the phase shift δ_0. Again we have $U(r)=0$ and $V(r)=V_{\delta-}(r)$ for $\delta_0 > 0$, and $U(r)=V_{\delta-}(r)$ and $V(r)=-V_{\delta-}(r)$ for $\delta_0 < 0$. Recoil energies must be determined numerically for $N=5000$ and are given in Table I. In Fig. 5 we show the XPS recoil profile for various values of the phase shift δ_0. For a given value of the phase shift these profiles again depend only on a/r_S, and we have $a/r_S = 0.14 a_B$, $0.18 a_B$, and $0.047 a_B$ for $\delta_0/\pi = 0.25$, 0.50, and 0.75, respectively.

These profiles are similar to the ones obtained for the square well potential of the previous subsection, and the same comments apply. The only difference is that in the case of the δ shell potential we can have at most one bound state.

D. Repulsive δ shell

The last form of the final-state interaction we have considered is the repulsive δ shell $V_{\delta+}(r)$ given by

$$V_{\delta+}(r) = V_0 a\,\delta(r-a). \tag{3.10}$$

Again we choose $V_0 a = 1.5 a_B$ Ry for $|\delta_0/\pi| \leq 0.5$ and $V_0 a = 6.0 a_B$ Ry for $|\delta_0/\pi| = 0.75$, after which the radius a is determined by the phase shift. For $\delta_0 > 0$ we have $U(r) = V_{\delta+}(r)$ and $V(r) = -V_{\delta+}(r)$ in Eqs. (1.1) and (1.2), while for $\delta_0 < 0$ we have $U(r)=0$ and $V(r)=V_{\delta+}(r)$. Recoil energies were again evaluated numerically and are given in Table I. In Fig. 6 we give the calculated XPS profiles for various values of δ_0. For $\delta_0 > 0$ the profiles are qualitatively (but not quantitatively) very similar to the corresponding profiles obtained for the repulsive barriers and the same general comments apply. For $\delta_0 < 0$ these profiles show a new feature, namely, a resonance, corresponding to an electron momentarily trapped within the barrier; similar resonances for d waves are common in transition metals.

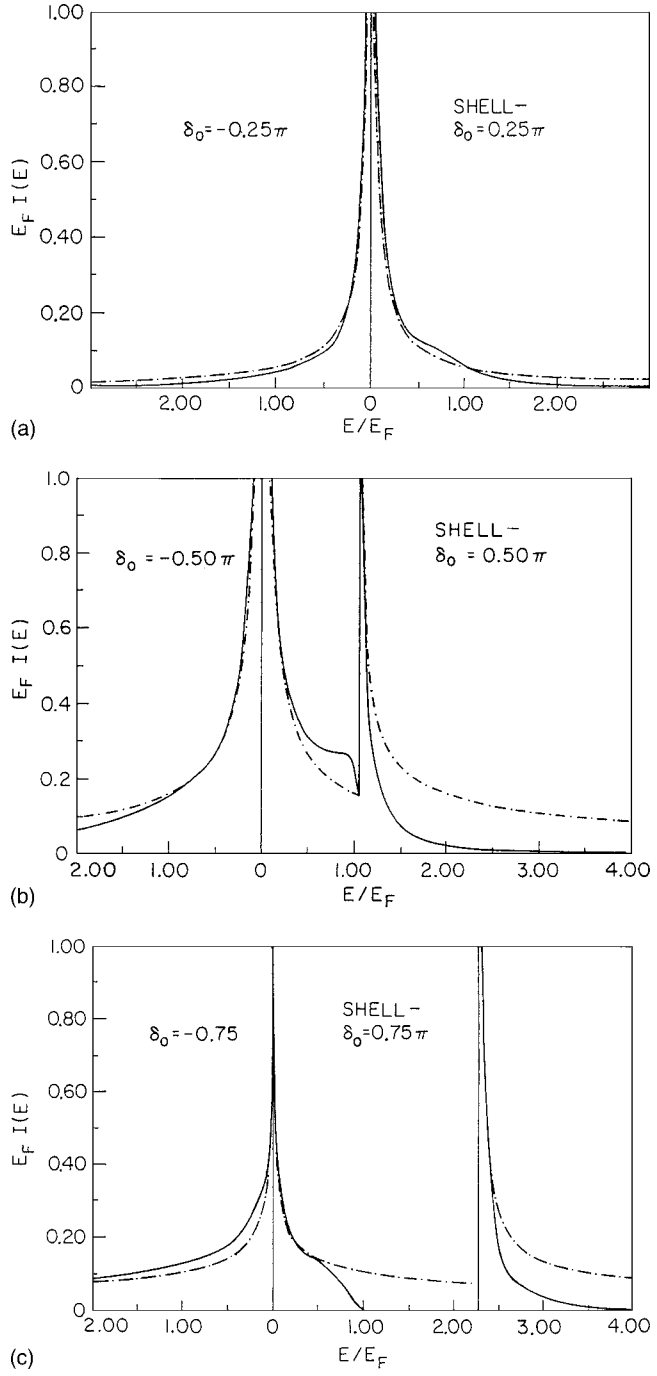

FIG. 5. Recoil profiles $E_F I(E)$ for turning on ($\delta_0 > 0$) and off ($\delta_0 < 0$) an attractive δ shell. The calculations have employed $a/r_s = 0.14a_B$, $0.18a_B$, and $0.047a_B$ for $\delta_0/\pi = 0.25$, 0.50, and 0.75 respectively, as in Fig. 3.

IV. X-RAY ABSORPTION AND EMISSION

A. Exact solutions for finite numbers of electrons

In the case of x-ray absorption and emission processes the number of electrons in the conduction band changes, and instead of calculating the overlap between the initial state and the various final states one now has to evaluate the dipole matrix element between the initial and the final states. To see how the calculations are carried out in this case, we first consider the x-ray absorption process. During this process, an electron, originally in the core state $|\phi_c\rangle$ centered at the origin, is injected into the conduction band by the absorption of a photon. We again use the Hamiltonians H_{initial} and H_{final} as given in Eqs. (1.1) and (1.2) for the initial and final states, but now we have $M = N+1$ in Eq. (1.2), i.e., in the final state the conduction band contains one more conduction electron than in the initial state. For simplicity we consider the case where the core state has angular momentum $\ell = 1$ (a p state) and we neglect exchange between the core state and the conduction band and exchange transitions[107] involving higher-angular-momentum electron states of the conduction band. (In principle exchange can be taken into account with our methods, but the calculations would become lengthier.) The final state contains either an additional s electron (s-wave channel) or an additional d electron (d-wave channel). Here we shall neglect the d-wave channel and consider only the physically interesting s-wave channel (for a core state with a very small radius the d-wave channel will give very small contributions).

The initial and final states are now given by $|i\rangle = |\phi_c\rangle|\Phi\rangle$ and $|f\nu\rangle$, respectively, where $|\Phi\rangle$ is a Slater determinant of N one-electron states $|\phi_n\rangle$ of H_{initial} and $|f\nu\rangle$ is a Slater determinant of $N+1$ single-particle states $|\psi_m\rangle$ of H_{final}. The absorption profile $\kappa(E)$ can now be written as

$$\kappa(E) = \sum_{f\nu} |\langle i|M|f\nu\rangle|^2 \delta(E - E_{f\nu} + E_i), \tag{4.1}$$

where $M = \Sigma_{j=1}^{N+1} z_j$ is the dipole operator and $E_{f\nu}$ and E_i are the total energies of the final and initial $(N+1)$-particle states. The matrix element $\langle i|M|f\nu\rangle$ can again be written as a determinant,

$$\langle i|M|f\nu\rangle = \begin{vmatrix} (\phi_c|z|\psi_j) & (\phi_c|z|\psi_\ell) & \cdots & (\phi_c|z|\psi_n) \\ (\phi_1|\psi_j) & (\phi_1|\psi_\ell) & \cdots & (\phi_1|\psi_n) \\ \cdots & & & \\ \cdots & & & \\ \cdots & & & \\ (\phi_N|\psi_j) & (\phi_N|\psi_\ell) & \cdots & (\phi_1|\psi_n) \end{vmatrix}, \tag{4.2}$$

where the occupied final-state single-particle orbitals are $|\psi_j\rangle, |\psi_\ell\rangle, \ldots, |\psi_n\rangle$. For a spherically symmetric system with $|\phi_c\rangle$ at its center and with isotropic potentials $U(r)$ and $V(r)$ at its center, the total absorption profile is a multiple convolution of the absorption profile in one channel (here the s-wave channel, spin up) and the XPS recoil profiles in all the remaining channels, so that we can again consider each channel separately, and in what follows we shall consider the single-spin s-wave absorption profile by itself.

If the core state $|\phi_c\rangle$ is known, the absorption profile $\kappa(E)$ can be evaluated for a finite number of electrons in essentially the same way as the XPS recoil profiles were evaluated (see below). Although it would be possible to use a realistic wave function for the core orbital of a specific metal, we have instead attempted to present the theory in a manner that does not depend on a specific material. Therefore, we make

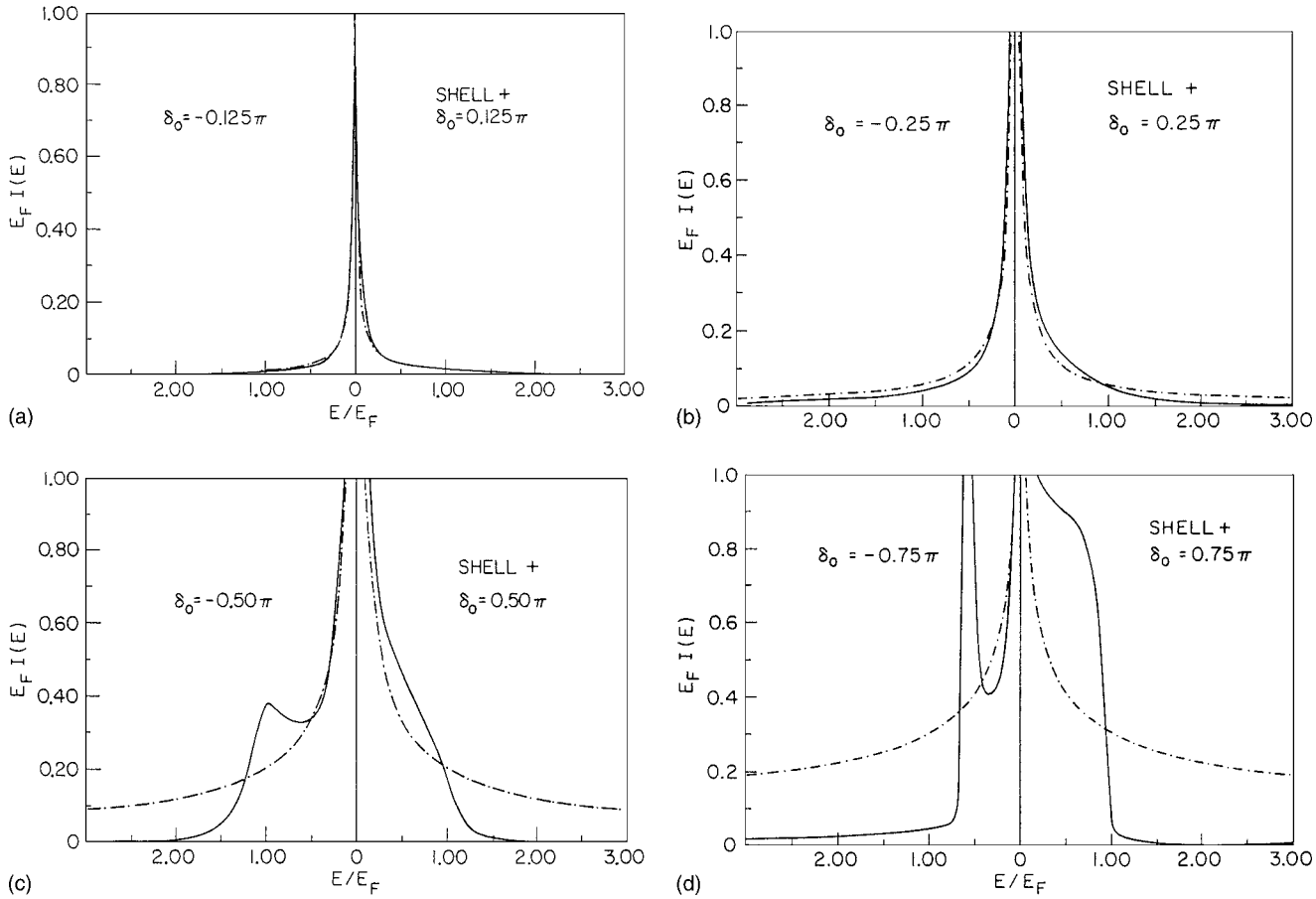

FIG. 6. Recoil profiles $E_F I(E)$ for turning on ($\delta_0 > 0$) and off ($\delta_0 < 0$) a repulsive δ shell. The calculations have employed $a/r_s = 0.32a_B$, $0.55a_B$, $1.00a_B$, and $1.27a_B$ for $|\delta_0|/\pi = 0.125$, 0.25, 0.50, and 0.75 respectively. As in Fig. 3.

the *small-core approximation*, namely, we assume that the core p state has a negligible radius a_c. This simplifies the expression for the matrix element considerably, since we can now write

$$\langle i|M|f\nu\rangle = M \begin{vmatrix} \psi_j(0) & \psi_\ell(0) & \cdots & \psi_n(0) \\ (\phi_1|\psi_j) & (\phi_1|\psi_\ell) & \cdots & (\phi_1|\psi_n) \\ \cdots & & & \\ \cdots & & & \\ \cdots & & & \\ (\phi_N|\psi_j) & (\phi_N|\psi_\ell) & \cdots & (\phi_1|\psi_n) \end{vmatrix}, \tag{4.3}$$

where the reduced matrix element M is given by[145]

$$M = (\phi_c|z|\psi_m)/\psi_m(0) = 48(\alpha^7/3)^{1/2}(\alpha^2 - k^2)/(\alpha^2 + k^2)^4. \tag{4.4}$$

This reduced matrix element depends on the core radius $a_c = 1/\alpha = a_B/Z_{\text{eff}}$, where a_B is the Bohr radius and Z_{eff} is the effective nuclear charge. For a hydrogen $2p$ state we have $M \to a_c^{5/2}$. The small-core approximation to the lineshape is valid for all energies such that $ka_c \ll 1$, where $\hbar^2k^2/2m$ is the kinetic energy of the optical electron. The small-core approximation breaks down at an electron energy of order Z_{eff}^2 Ry. Figure 7 displays this effect for various values of the core radius a_c.

The spectra are now calculated for an $(N+1)$-electron system by going through the same steps as were described for the XPS case in Sec. II A, the only difference being that the first row of the determinant of overlaps is now replaced by the appropriate final state orbitals evaluated at $r=0$. The calculated spectra $Y(E)$ for $N=5$, 10, 20, 40, and 80 show again the stability of the profile against changes in the number of electrons (see Fig. 8).

The case of x-ray emission is slightly different from absorption, since now the initial state $|i\rangle$ contains $N+1$ conduction electrons in the presence of the core hole and the final states $|f\nu\rangle$ contain N conduction electrons and the core p electron. If we denote the single-particle conduction orbitals in the initial state by $|\psi_m)$ and those in the final state by $|\phi_n)$, we obtain the same result for $\langle i|M|f\nu\rangle$ as given by Eqs. (4.1) and (4.3) for absorption. The difference between absorption and emission lies in the fact that for absorption the orbitals $|\psi_m)$ are different in the various final states $|f\nu\rangle$, whereas for emission the orbitals $|\phi_m)$ are different in the various final states. [So for emission the first row of the determinant of Eq. (4.3) is the same for all final states.]

Just as in the case of the XPS spectra, there are some useful checks on the calculations. First consider the case of x-ray emission. Here we have for the integrated spectrum

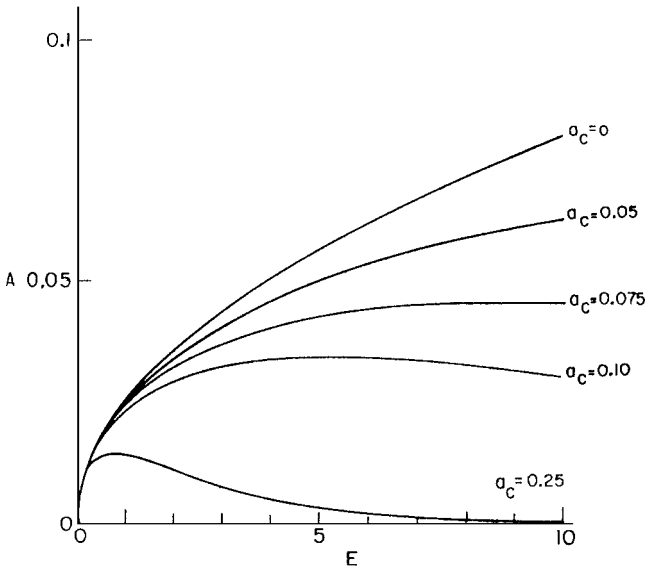

FIG. 7. Plot of $A=(\pi^2/192)(M^2/a_c^5)E^{1/2}$ versus energy for various values of the core radius a_c, showing the falloff of the free-electron square root caused by the finite core radius. A is given by [compare with Eq. (4.4)] $A=(1-a_c^2E)^2(1+a_c^2E)^{-8}(E^{1/2}/4\pi^2)$.

$$J(\infty)=\sum_{f\nu}|\langle i|M|f\nu\rangle|^2$$
$$=\sum_{j<\cdots<n<i}\begin{vmatrix}(\phi_c|z|\psi_1) & (\phi_c|z|\psi_2) & \cdots & (\phi_c|z|\psi_{N+1})\\ (\phi_j|\psi_1) & (\phi_j|\psi_2) & \cdots & (\phi_j|\psi_{N+1})\\ \cdots & & & \\ \cdots & & & \\ \cdots & & & \\ (\phi_n|\psi_1) & (\phi_n|\psi_2) & \cdots & (\phi_n|\psi_{N+1})\end{vmatrix}^2. \tag{4.5}$$

Now we expand the determinant with respect to the first row. Note that the minors $M_{1,q}$ of the first row now represent overlaps of two N-electron states; in this overlap the initial state is made up out of all the initial one-electron orbitals except $|\psi_q\rangle$, and the final state is made up out of the same one-electron continuum states as in the original determinant. Assuming that the initial states can be expanded in a complete set of final continuum states, we can carry out the sum and obtain

$$J(\infty)=\sum_{j=1}^{N+1}|(\phi_c|z|\psi_j)|^2=M^2\sum_{j=1}^{N+1}|\psi_j(0)|^2. \tag{4.6}$$

Due to the small-core approximation, there exists no sum rule for the x-ray absorption profile. However, in this case it is possible to obtain the behavior of the profile far away from threshold, where the spectrum approaches screened-exciton theory. In order to describe this asymptotic behavior it is convenient to first consider the screened-exciton approximation, which will be done in the next subsection.

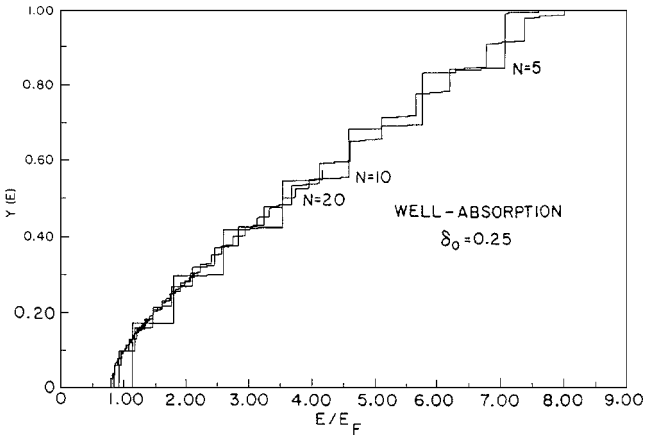

FIG. 8. Integrated absorption spectrum $Y(E)$ for a square well with $\delta_0=0.25\pi$ with $\delta_0=0.25\pi$ versus energy in units of the Fermi energy, for $N=5$, 10, 20, 40, and 80.

B. Screened-exciton approximation

As follows from Flynn's derivation of the XPS line shape, which contains no explicit information about the excited states, the ND theory is an asymptotic theory, valid only close to threshold. The question arises whether away from threshold the line shape can be described by some other simple approximation. As will be shown below, the gross features of the spectra far from threshold are very well described by screened-exciton theory,[62,75] which we shall now describe.

Screened-exciton theory (SEA) starts out by using the same expression for the absorption and emission profiles as one obtains with one-electron theory,

$$\kappa_{\mathrm{SEA}}(E)=\sum_m|(\phi_c|z|\psi_m)|^2\delta(E-E_m), \tag{4.7}$$

but rather than using the unperturbed one-electron wave functions $|\phi_m\rangle$, screened-exciton theory uses the perturbed wave functions $|\psi_m\rangle$; i.e., the screened-exciton approximation produces the spectrum one would obtain if the optical electron experienced the screened potential of the core hole, but the conduction electrons did not recoil during the transition. Here we shall apply screened-exciton theory to the case where no potential is present when the core state $|\phi_c\rangle$ is filled. [This means that we shall always have $U(r)=0$ in Eq. (1.1) when dealing with absorption, and $U(r)=W(r)$, $V(r)=-W(r)$ in Eqs. (1.1) and (1.2) when dealing with emission. Here $W(r)$ is the particular interaction we are considering. In other words, for absorption the wave functions $|\psi_m\rangle$ in Eq. (4.7) are the final-state single-particle wave functions, while for emission they are the initial-state wave functions.] We now make the same small-core approximation in Eq. (4.7) as was done to obtain Eq. (4.3), which leads to

$$\kappa_{\mathrm{SEA}}(E)=M^2\sum_m|\psi_m(0)|^2\delta(E-E_m). \tag{4.8}$$

For an attractive final-state interaction, excess charge will be localized near the core hole, so that $|\psi_m(0)|$ will be greater than the free-electron wave function evaluated at $r=0$. This

means that for an attractive final-state interaction screened-exciton theory predicts an enhancement of the free-electron profiles. This will be worked out below for a square well and an attractive δ shell, but first we shall consider the behavior of the absorption profile far away from threshold.

As we already mentioned in Sec. IV A, there exists no sum rule for the absorption profile, due to the small-core approximation (4.4). However, it is possible to obtain the behavior of the absorption profile far away from threshold. To see this we consider again

$$\kappa(E) = M^2 \sum_{j<1<\cdots<n} \begin{vmatrix} \psi_j(0) & \psi_1(0) & \cdots & \psi_n(0) \\ (\phi_1|\psi_j) & (\phi_1|\psi_1) & \cdots & (\phi_1|\psi_n) \\ \cdots & & & \\ \cdots & & & \\ \cdots & & & \\ \cdots & & & \\ (\phi_N|\psi_j) & (\phi_N|\psi_1) & \cdots & (\phi_N|\psi_n) \end{vmatrix} \times \delta(E - E_{f\nu} + E_i), \tag{4.9}$$

and let n become very large. Since $\psi_n(0)$ is proportional to k_n and, for large n, $(\phi_j|\psi_n)$ is inversely proportional to k_n, we see that if we expand the determinant with respect to the last column, we can write the determinant as

$$\psi_n(0) \begin{vmatrix} (\phi_1|\psi_j) & \cdots & \cdots & (\phi_1|\psi_{N-1}) \\ (\phi_2|\psi_j) & \cdots & \cdots & (\phi_2|\psi_{N-1}) \\ \cdots & & & \\ \cdots & & & \\ \cdots & & & \\ (\phi_N|\psi_j) & (\phi_N|\psi_1) & \cdots & (\phi_m|\psi_{N-1}) \end{vmatrix}. \tag{4.10}$$

Now suppose that both n and $N-1$ become very large. Then the last column of the determinant in Eq. (4.10) consists of only zeros and this contribution vanishes. This means that for large energies E we can write

$$\begin{aligned} \kappa(E) &= M^2 \sum_{j<\cdots<n} |\psi_n(0)|^2 \begin{vmatrix} (\phi_1|\psi_j) & \cdots & \cdots & (\phi_1|\psi_{N-1}) \\ (\phi_2|\psi_j) & \cdots & \cdots & (\phi_2|\psi_{N-1}) \\ \cdots & & & \\ \cdots & & & \\ \cdots & & & \\ \cdots & & & \\ (\phi_N|\psi_j) & \cdots & \cdots & (\phi_N|\psi_{N-1}) \end{vmatrix} \\ &\quad \times \delta(E - E_{f\nu} + E_i) \\ &= M^2 \int d\epsilon \sum_n |\psi_n(0)|^2 \delta(E - \epsilon - \epsilon_n) \\ &\quad \times \sum_{j<\cdots<N-1} |\langle i|f\nu'\rangle|^2 \delta(\epsilon - E_{f\nu'} + E_i) \\ &= \int d\epsilon\, \kappa_{\mathrm{SEA}}(E - \epsilon) I(\epsilon). \end{aligned} \tag{4.11}$$

Here $\langle i|f\nu'\rangle$ is the overlap of the initial N-particle state made up out of $|\phi_1\rangle, \ldots, |\phi_N\rangle$ and the final N-particle state, which has the state $|\psi_n\rangle$ missing from the original $(N+1)$-particle state. $E_{f\nu'}$ is the total energy of the N-particle final state, $\kappa_{\mathrm{SEA}}(E)$ is the absorption profile given by the screened-exciton approximation [see Eq. (4.8)], and $I(\epsilon)$ is the XPS recoil profile. In most cases, the recoil profile $I(\epsilon)$ becomes zero for $\epsilon \approx E_F$, so that ϵ is always small compared to E in Eq. (4.11). We may then expand $\kappa_{\mathrm{SEA}}(E-\epsilon)$ in a Taylor series around E, and if we cut off this series after the first term, we obtain

$$\kappa(E) \approx \kappa_{\mathrm{SEA}}(E) \quad \text{as } E \to \infty. \tag{4.12}$$

Thus for large energies the absorption profile should approach the spectrum given by the screened-exciton approximation. This is indeed borne out by the calculations, as will be shown in Sec. V.

We now return to the discussion of screened-exciton theory itself, which was interrupted after Eq. (4.8). If we enclose our system in a box of radius R and let $R \to \infty$, we may replace the sum over n by $(R/\pi)\int dk$, which gives

$$\kappa_{\mathrm{SEA}}(E) = (RM^2/\pi) \int dk |\psi_k(0)|^2 \delta(E - k^2). \tag{4.13}$$

We will work out this expression for the square well and the attractive δ shell. (For the normal case where $\delta_0 > 0$ in absorption, the screened-exciton theory reduces to the free-electron theory for the repulsive final-state interactions of the infinite barrier and the repulsive δ shell. See, however, Sec. VI for an application of screened-exciton theory to the case of the repulsive δ shell for $\delta_0 < 0$.)

1. Square well

In this case we need to solve for the one-electron states of the potential $V_W(r)$, given by Eq. (3.3). The solutions are

$$|\psi) = (2\pi R r^2)^{-1/2} \sin(kr + \delta_k), \quad r > a, \tag{4.14}$$

and

$$|\psi) = (2\pi R r^2)^{-1/2} \sin(ka + \delta_k) \sin(\kappa r)/\sin(\kappa a), \quad r < a. \tag{4.15}$$

Here we have $k^2 = E$ and $\kappa^2 = V_0 + E$. We find for $|\psi(0)|^2$

$$|\psi(0)|^2 = \kappa^2 \sin^2(ka + \delta_k)/(2\pi R \sin^2 \kappa a). \tag{4.16}$$

The phase shift δ_k may be eliminated from Eq. (4.16) by using the continuity of $d\psi/dr$ at $r=a$, which gives

$$\cot(ka + \delta_k) = (\kappa/k)\cot(\kappa a). \tag{4.17}$$

With this result we can write

$$|\psi(0)|^2 = k^2\kappa^2/2\pi R(k^2 + V_0 \cos^2 \kappa a), \tag{4.18}$$

and substitution of Eq. (4.18) into Eq. (4.13) finally gives

$$\kappa_{\mathrm{SEA}}(E) = M^2(E^{1/2}/4\pi^2)(E + V_0)/ [E + V_0 \cos^2 a(E + V_0)^{1/2}]. \tag{4.19}$$

This expression describes emission for $E < E_F$ and absorption for $E > E_F$. We see that the free-electron square root

behavior is enhanced by a factor $((E+V_0)/[E+V_0\cos^2 a(E+V_0)^{1/2}]$.

2. Attractive δ shell

In this case the potential is given by $V_\delta-(r)=-V_0a\delta(r-a)$ and the s states of the system are

$$|\psi\rangle = (2\pi Rr^2)^{-1/2}\sin(kr+\delta_k), \quad r>a, \tag{4.20}$$

and

$$|\psi\rangle = (2\pi Rr^2)^{-1/2}\sin(ka+\delta_k)\sin(kr)/\sin(ka), \quad r<a. \tag{4.21}$$

We use the integrated Schrödinger equation

$$k\sin(ka+\delta_k)\cos(ka) = V_0a\sin(ka+\delta_k)\sin(ka) + k\cos(ka+\delta_k)\sin(ka) \tag{4.22}$$

to eliminate the phase shift from the expression for $|\psi(0)|^2$, and obtain

$$|\psi(0)|^2 = k^4/(2\pi R)(k^2-2kV_0a\sin(ka)\cos(ka) + (V_0^2a^2\sin^2 ka)). \tag{4.23}$$

Substitution of Eq. (4.23) into Eq. (4.13) gives

$$\kappa_{\mathrm{SEA}}(E) = M^2(E^{1/2}/4\pi^2)\{E/[E-2kV_0a\sin(ka)\cos(ka) + V_0^2a^2\sin^2 ka]\}, \tag{4.24}$$

where we have $k^2=E$. Again the free-electron square-root-of-energy behavior is enhanced, now by the factor in braces in Eq. (4.24).

C. Limit of infinite number of electrons

To obtain the behavior of the absorption and emission profiles from the numerical profiles as $N\to\infty$, we formally use an expression similar to Anderson's theorem, but now for $|\langle i|M|f0\rangle|^2$. We write

$$|\langle i|M|f0\rangle|^2 = M^2CN^{-\Delta}, \tag{4.25}$$

where the exponent is given by

$$\Delta = (\delta_0/\pi-1)^2 \tag{4.26}$$

appropriate for absorption or emission.[48,49] The constant C is obtained from

$$C = \lim_{N\to\infty}|\langle i|M|f0\rangle|^2N^{\Delta}/M^2. \tag{4.27}$$

The calculated lines (integrated spectra) are now fitted with an expression of the form

$$J(x) = C(x/2)^{\Delta(x)} \tag{4.28}$$

just as in the case of the XPS profiles, with $\Delta(x)=\Delta+\Sigma_{p=1}^{5}a_px^p$. Again this expression is valid only for $x<2$, and away from threshold we have to use a different expression. For the case of absorption we have seen that far away from threshold the exact profile should approach the screened-exciton profile, which is expected to depend on the energy through a factor $E^{1/2}$ [see Eqs. (4.19) and (4.24)], just like the free-electron profile. Therefore, the calculated absorption line shapes (integrated spectra) are fitted with an expression of the form

$$J(x) = \sum_{p=0}^{4} c_px^{p+1/2} \tag{4.29}$$

far away from threshold $\left(x>\frac{1}{2}\right)$.

In the case of emission one might expect to be able to use the sum rule Eq. (4.6) again and fit the integrated spectrum with a function of the type given in Eq. (2.13). Unfortunately, the sum rules depend weakly on the number of particles in this case and are of little use in determining small contributions to $\kappa(E)$ far away from threshold. However, it turns out that the sum rules for finite N are already almost saturated for $E\approx E_F$, and it is possible to obtain an accurate fit to the line shape $\kappa(E)$ by convolving the numerical spectra with a Gaussian of width comparable to the level spacing, just as described in Sec. II B for the XPS spectra. The absorption spectra were also broadened with Gaussians as a check of the fit and to remove any ambiguities in the region where the two fits overlap.

V. RESULTS FOR ABSORPTION AND EMISSION PROFILES

In this section we shall give the results of our calculations for the case where $\delta_0>0$ in absorption, i.e., the state with the core hole present always has a more attractive potential than the state in which the core hole is filled. This case is the most appropriate one to consider for x-ray absorption and emission.

We have again considered four forms for the final-state interaction, which will be discussed separately Secs. V A–V D. No recoil energies will be given for these cases, since the recoil energies for absorption are related simply to the recoil energies for XPS ($\delta_0>0$) by

$$E_R^{\mathrm{ABS}} - E_R^{\mathrm{XPS}} = E_F. \tag{5.1}$$

So the recoil energies can easily be obtained from those given in Table I for XPS.

A. Repulsive barrier

Here we use again $V_B(r)=\infty$ for $r<a$, $V_B(r)=0$ for $r>a$, where a is determined by the phase shift at the Fermi level. For absorption we have $U(r)=V_B(r)$, $V(r)=-V_B(r)$ in Eqs. (1.1) and (1.2), while for emission we have $U(r)=0$, $V(r)=V_B(r)$. The recoil energies can again be calculated exactly in this case and are given by

$$E_R = E_F - (2\delta_0/3\pi)E_F. \tag{5.2}$$

The sum rule for the case of emission, Eq. (4.6), can also be evaluated exactly in this case and gives

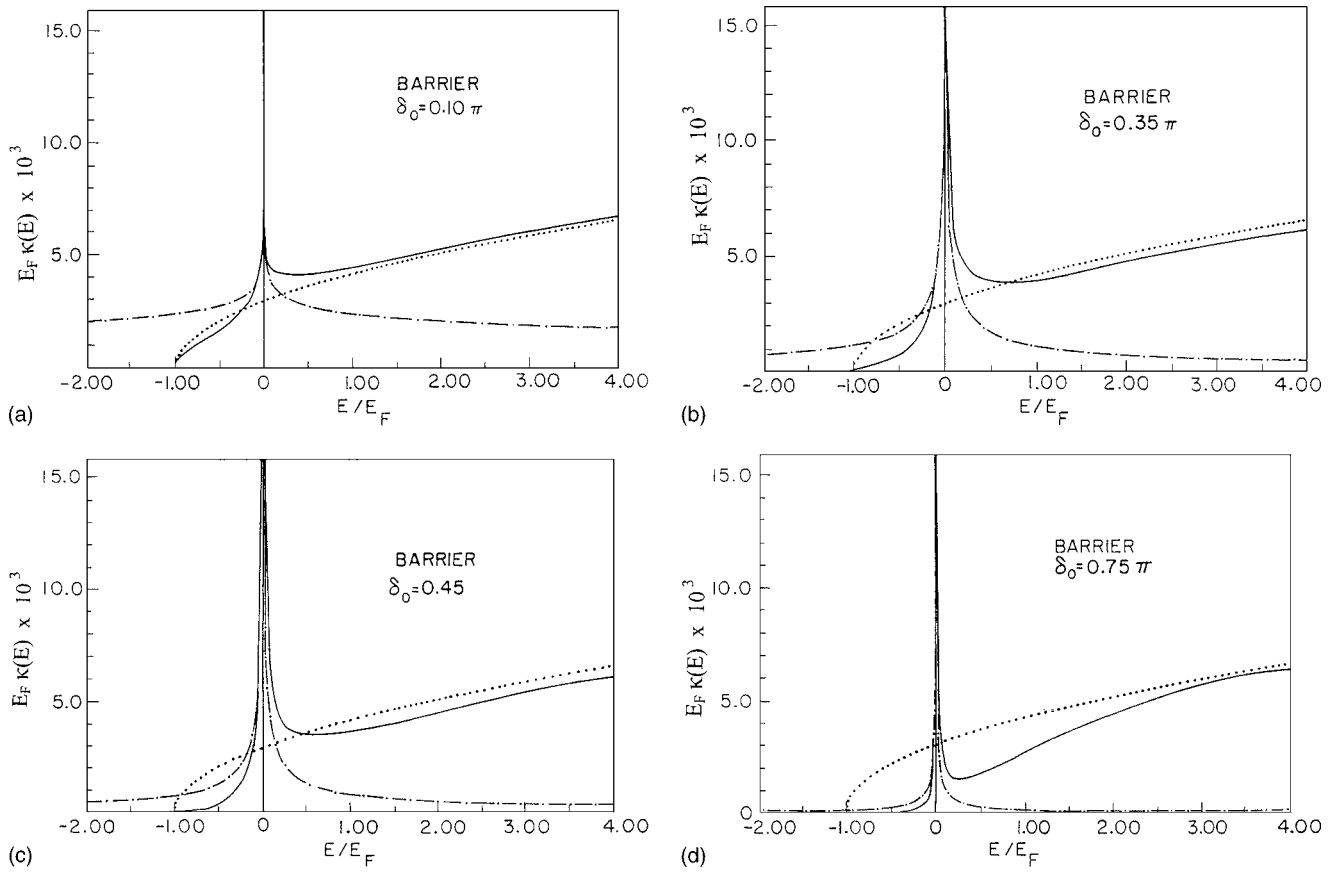

FIG. 9. Emission and absorption profiles $E_F\kappa(E)/M^2$ for a barrier of infinite height. Emission profiles are displayed to the left of the common threshold, absorption profiles to the right. Solid lines, exact results; chained lines, ND theory; dotted lines, free-electron theory. Not in this figure, but in some of the following figures, broken lines, screened-exciton approximation.

$$J(\infty)/M^2 = \sum_{n=1}^{N+1} k_n^2/2\pi R$$
$$= \pi(N+1)(N+2)(2N+3)/12R^3$$
$$= (k_F^3/6\pi^2)(N+1)(N+2)(2N+3)/(N+1)^3. \quad (5.3)$$

For $N\to\infty$ we find

$$J(\infty)/M^2 = k_F^2/6\pi^2. \quad (5.4)$$

In Fig. 9 we show the x-ray absorption and emission profiles obtained for various values of δ_0. The common threshold is set equal to zero and emission appears for negative energies, absorption for positive energies. Also shown in the figures are the ND profiles (chained) and the free-electron profiles (dotted). In this case the screened-exciton approximation reduces to the free-electron result and is not shown. The exact curve clearly shows the threshold anomaly, which arises from interferences inherent in the determinantal wave functions, as demonstrated by Friedel.[43,44,48] We see again that the exact results start to deviate from the ND curve very close to threshold ($|E-E_T| > \approx 0.03E_F$). For small phase shifts the spectra are very well described by the screened-exciton approximation (free-electron curves), except close to threshold. For larger phase shifts we see that the absorption profile does indeed approach the screened-exciton result far away from threshold. Deviations from the screened-exciton theory are most pronounced near threshold, where the screened-exciton theory cannot produce an edge anomaly, and, in emission, above the bottom of the band, where the sum rule causes a depletion of the emission profile that compensates the edge anomaly. For larger phase shifts there is a similar effect in absorption just above threshold, where the exact profile dips below the screened-exciton profile in an apparent attempt to make up for the edge anomaly. It is also clear that the absorption and emission profiles are not mirror images of each other, except very close to threshold.

Absorption and emission edges which are not mirror symmetric have been reported.[8] Such behavior is to be expected on the basis of the present work.

As the phase shift increases, the divergence at the threshold becomes more pronounced [$(\delta_0/\pi-1)^2\to 0$ as $\delta_0/\pi \to 1$], in contrast with the behavior of the XPS profiles.

B. Attractive square well

1. Spectra

Here we use again $V_W(r)=-V_0\theta(a-r)$. We arbitrarily choose $a=1.5a_B$, after which the strength V_0 is determined by the phase shift at the Fermi level. For absorption we have $U(r)=0$, $V(r)=V_W(r)$ in Eqs. (1.1) and (1.2), while for emission we have $U(r)=V_W(r)$, $V(r)=-V_W(r)$. In Fig. 10 we show

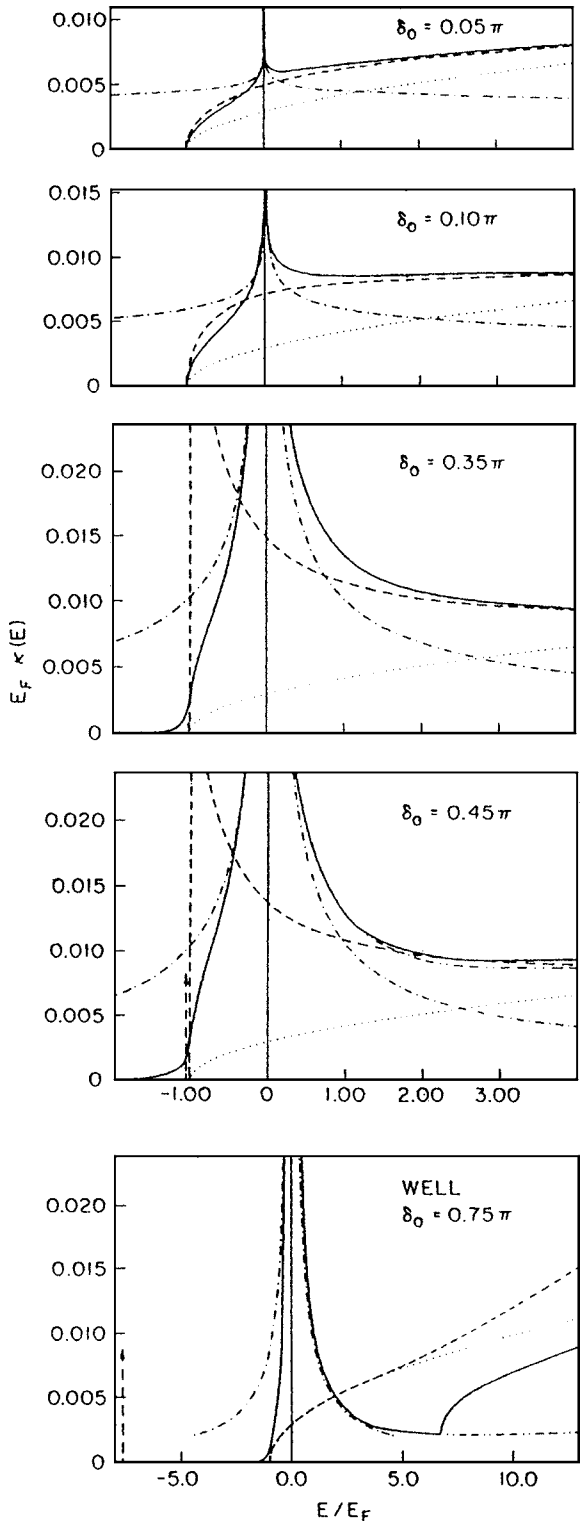

FIG. 10. Emission and absorption profiles $E_F\kappa(E)/M^2$ for a square well of width $a=1.5a_B$ $(a/r_s=0.38a_B)$; as in Fig. 9.

the absorption and emission profiles for various values of δ_0. Also shown are the normalized ND result, the free-electron result, and the screened-exciton profile, as obtained from Eq. (4.19). For small phase shifts we see again that the exact profile is very well described by screened-exciton theory, except very close to threshold, and that screened-exciton theory does indeed give an enhancement of the free-electron result, as predicted in Sec. IV B. It is also clear that the ND result agrees only very close to threshold with the exact solutions, and that the absorption and emission profiles are not mirror images. For $\delta_0>0.38\pi$ a second threshold appears in the absorption spectra, due to the fact that the potential is now strong enough to produce a bound state. The profile does not diverge at this second threshold, but instead vanishes with an exponent $(\delta_0/\pi-2)^2$, in agreement with the predictions of Combescot and Nozières[53] (see also Ref. 49). Due to the fact that screened-exciton theory does not take the relaxation of the conduction electrons into account properly, the screened-exciton profile seems widely different from the exact profile. However, if we take this electronic relaxation into account by shifting the screened-exciton profile to the right over a distance of $E_F+\epsilon_B$, to make the continuum absorption thresholds agree for the two cases, it will be seen that the screened-exciton profile once again agrees very well with the exact profile. The deviations of screened-exciton theory from the exact result in emission for $\delta_0=0.35\pi$ is related to the same recoil energy problem.

2. Evolution of the spectra from the free-electron limit to the exciton limit

Figure 10 shows how the absorption and emission spectra behave as the strength of the final-state interaction increases from zero to a magnitude sufficient to produce a bound exciton. The spectra evolve from the square-root-of-energy shape of free-electron theory to the characteristic exciton shape.

C. Attractive δ shell

In this case we use again $V_{\delta-}(r)=-V_0a\delta(r-a)$ and let $U(r)=0$, $V(r)=V_{\delta-}(r)$ in Eqs. (1.1) and (1.2) for absorption, while for emission we have $U(r)=V_{\delta-}(r)$, $V(r)=-V_{\delta-}(r)$. The profiles obtained for this case are shown in Fig. 11. These profiles are qualitatively similar to those obtained for the square well, but the enhancement factor in screened-exciton theory is larger in this case. The same comments apply for the case of the attractive δ shell as were made for the square well.

D. Repulsive delta shell

Here we use $V_{\delta+}(r)=V_0a\delta(r-a)$ and let $U(r)=V_{\delta+}(r)$ in Eqs. (1.1) and (1.2) for absorption, while for emission we use $U(r)=0$, $V(r)=V_{\delta+}(r)$. The profiles obtained for this case are shown in Fig. 12. Again the screened-exciton theory reduces to the free-electron theory. The spectra are quite similar to those of the barrier and the same comments apply.

E. Comparison of barrier, well, and attractive shell

Figure 13 shows the absorption and emission spectra $E_F\kappa(E)/M^2$ for three different final-state interactions, all with $\delta_0=0.25\pi$. Although all have Nozières–de Dominicis peaks at the threshold, the strengths of the spectra and those peaks are quite different.

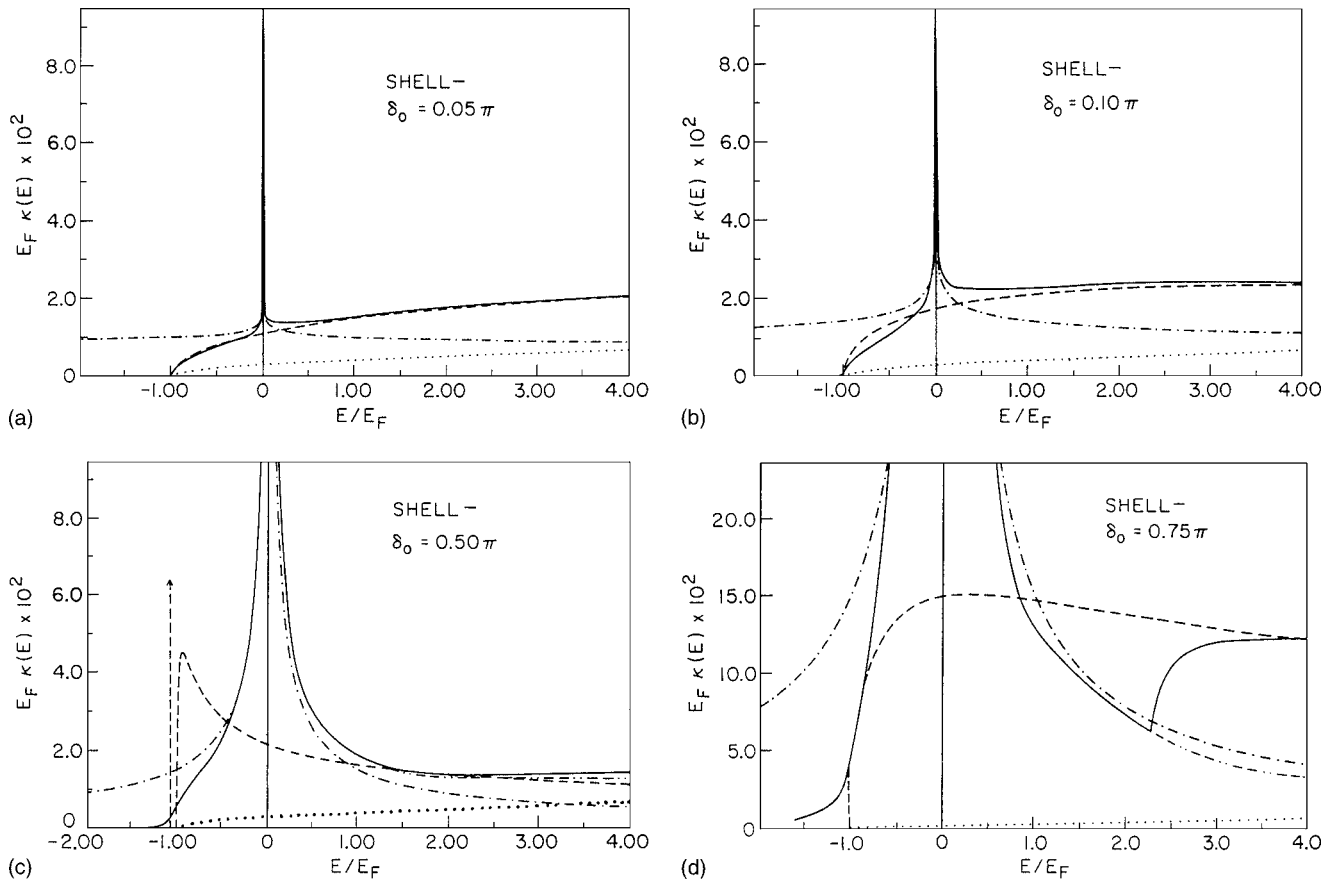

FIG. 11. Emission and absorption profiles $E_F\kappa(E)/M^2$ for an attractive δ shell. The calculations have employed $a/r_s=0.085a_B$, $0.11a_B$, $0.18a_B$, and $0.047a_B$ for $\delta_0/\pi=0.05$, 0.10, 0.50, and 0.75, respectively. As in Fig. 9.

VI. SUMMARY

In summary, we have employed a "change of mean-field model" and have shown that x-ray line shapes of metals can be rich in structure, depending on the final-state interactions. Much of this structure had been unanticipated in previous work.

Especially noteworthy are the qualitative features of the exact change of mean-field line shapes which offer possible explanations of current paradoxes: (i) the deviation of the exact theory from the asymptotic solution; (ii) the exhaustion of the XPS sum rule (2.7) at relatively low energies for some final-state interactions, which could lead to the observation of apparently symmetric lines; and (iii) the lack of mirror symmetry for absorption and emission edges.

The change of mean-field method can be adapted to treat final-state interactions in metals with band structure; the resulting calculations can be executed with contemporary desk-top computers. At the present, such an ambitious computational project seems unwarranted for the simple free-electron metals, because final-state interactions are rather weak and the form of the interaction for any specific metal is not well understood. But, for polyvalent metals and for metallic systems with strong final-state interactions, the finite-number-of-electrons method provides a powerful technique for understanding multielectron recoil.

ACKNOWLEDGMENTS

We gratefully acknowledge the support of the Department of Energy through the Illinois Materials Research Laboratory, and the support of the Office of Naval Research (Grant No. N00014-03-1-0375) and the U.S. Army Reseach Office (Grant No. W911NF-05-1-0346 ARO). We also thank C. P. Flynn and R. Naumann for many stimulating conversations.

APPENDIX: DETAILS OF THE CALCULATIONS

In this appendix we give some of the mathematical details of the calculations, such as the determination of the parameters of the final-state interaction, the form of the wave functions, and the number of bound states for the attractive potentials.

In all the cases that we have considered, we have a free-electron gas in either the initial or the final state, and it is for this state that we specify the electron density or radius parameter r_s, after which the Fermi wave vector follows as $k_F=k_F^0=(9\pi/4)^{1/3}/r_s a_B$ and the radius R of the system is given by $R=N\pi/k_F^0$. Here N is the number of s conduction electrons present in the state for which the core state is occupied. (In other words, for the square well and the attractive δ shell potentials we always use N electrons in the state with no potential present and $N+1$ electrons in the state with the

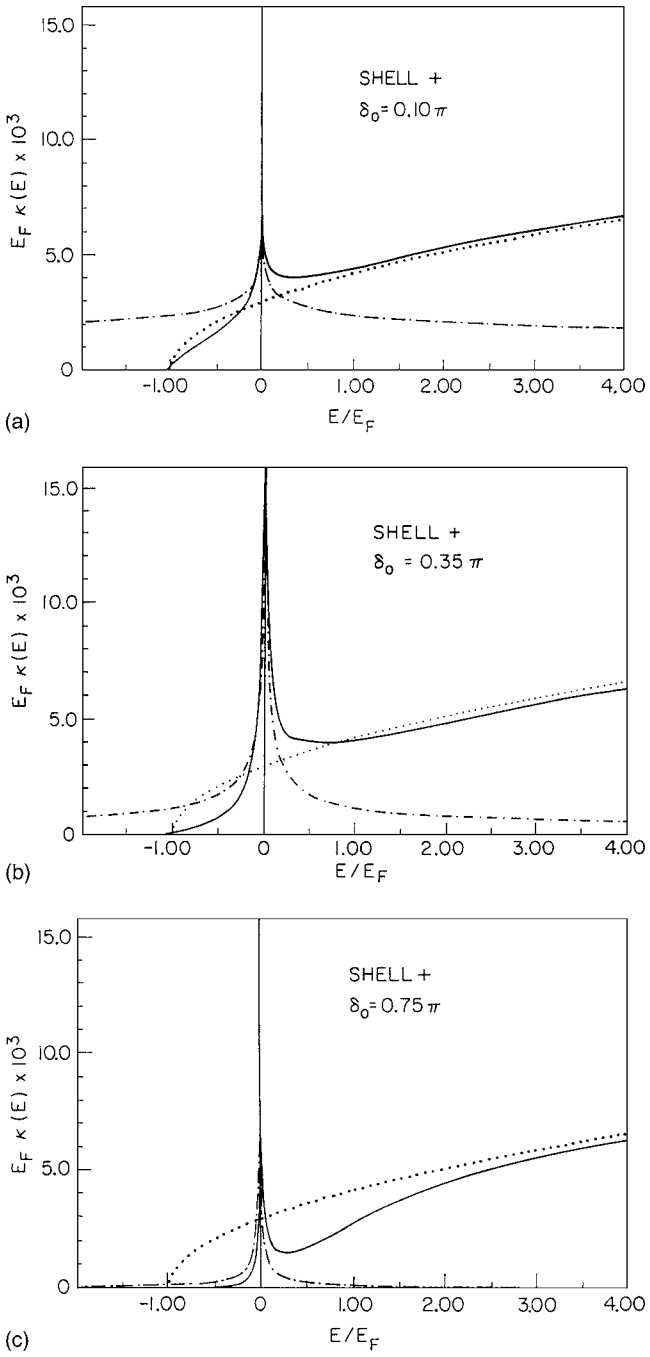

FIG. 12. Emission and absorption profiles $E_F\kappa(E)/M^2$ for a repulsive δ shell. The calculations have employed $a/r_s=0.27a_B$, $0.73a_B$, and $1.27a_B$ for $\delta_0/\pi=0.10$, 0.35, and 0.75 respectively. As in Fig. 9.

potential present. For the barrier and the repulsive shell, however, we use again N electrons for the state with no potential present, but $N-1$ electrons for the state with the potential present.)

The one-electron wave functions for the free-electron gas are given by

$$|\phi_n) = (2\pi R r^2)^{-1/2}\sin(k_n r), \quad k_n = n\pi/R. \tag{A1}$$

Here n can take on only integer values.

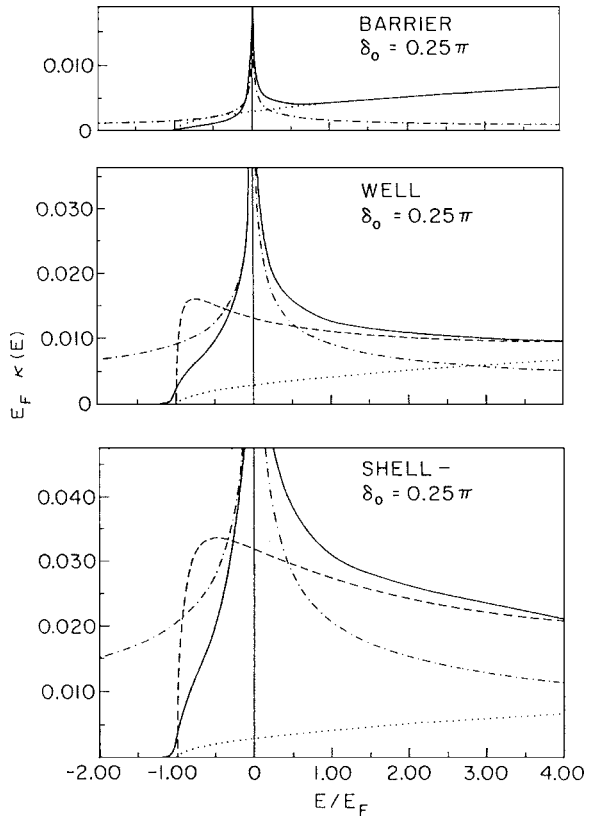

FIG. 13. Comparison of the absorption and emission spectra $E_F\kappa(E)/M^2$ for various potentials with $\delta_0=0.25\pi$, namely, barrier, square well, and attractive δ shell. As in Fig. 9.

In Secs. A 1–A 4 we discuss the various final-state interactions employed in this work.

1. Barrier

For an infinite barrier of radius a, the one-electron wave functions can be written as

$$|\psi_m) = [2\pi(R-a)r^2]^{-1/2}\sin[k'_m(r-a)],$$
$$k'_m = m\pi/(R-a), \quad a < r < R. \tag{A2}$$

For the wave function with energy equal to the (perturbed) Fermi energy we have

$$|\psi_F) \sim r^{-1}\sin(k'_F r - \delta_0) \tag{A3}$$

and the boundary condition at $r=R$ gives

$$k'_F R - \delta_0 = N\pi \rightarrow k'_F = (N\pi + \delta_0)/R = N\pi/(R-a), \tag{A4}$$

where the last step follows from Eq. (A2). From Eq. (A4) we obtain for the radius of the barrier

$$a = \delta_0/(k_F^0[1 + \delta_0/N\pi]). \tag{A5}$$

2. Square well

For a square well of strength V_0 and radius a (which we arbitrarily choose to be $1.5a_B$) the continuum wave functions can be written as

$$|\psi_m) = \begin{cases} A(\sin \kappa_m r)/(r \sin \kappa_m a), & r < a, \\ A[\sin k_m(R-r)]/[r \sin k_m(R-a)], & r > a. \end{cases} \tag{A6}$$

Here A is a normalization constant and we must have

$$k_m^2 = \epsilon_m, \quad \kappa_m^2 = k_m^2 + V_0, \tag{A7}$$

where ϵ_m is the energy eigenvalue of the wave function. If the strength V_0 of the potential is known, the allowed wave vectors follow from the boundary condition at $r=a$:

$$\kappa_m \cot(\kappa_m a) = -k_m \cot[k_m(R-a)]. \tag{A8}$$

Before determining the strength of the potential, we first obtain the perturbed Fermi wave vector k_F'. To do this we notice that the wave function with energy at the (perturbed) Fermi level can be written as

$$|\psi_F) = \begin{cases} A(\sin \kappa_F r)/(r \sin \kappa_F a), & r < a, \\ A \sin(k_F' r + \delta_0)/r \sin(k_F' a + \delta_0), & r > a. \end{cases} \tag{A9}$$

The perturbed wave vector k_F' at the perturbed Fermi level is now determined from the boundary condition at $r=R$:

$$\sin(k_F' R + \delta_0) = 0 \rightarrow k_F' = (N\pi - \delta_0)/R = k_F^0 - \delta_0/R, \tag{A10}$$

where k_F^0 is the unperturbed Fermi wave-vector.

From the boundary condition at $r=a$ we obtain

$$\tan x = (x/k_F' a)\tan(k_F' a + \delta_0), \tag{A11}$$

where we have written

$$x = \kappa_F a = a(V_0 + k_F'^2)^{1/2}. \tag{A12}$$

Equation (A11) can be solved for x, after which V_0 can be obtained from Eq. (A12). We notice that Eq. (A11) has a trivial solution $x=0$ which must be discarded, since it would lead to wave functions with zero amplitude inside the well. Furthermore, x is not determined uniquely by Eq. (A11). To get around this difficulty, we determine the interval n in which $(k_F' a = \delta_0)$ lies from

$$(n-1)\pi/2 < (k_F' a + \delta_0) < n\pi/2, \tag{A13}$$

and require $x = \kappa_F a$ to be in the same interval. This has the following advantages: (i) x is determined uniquely; (ii) $V_0 \rightarrow 0$ as the phase shift goes to zero; and (iii) V_0 increases continuously with increasing δ_0.

Once V_0 is determined, the allowed wave vectors for the continuum states are obtained by solving Eq. (A8) with the Newton-Raphson method.[146]

If the potential is strong enough, we can also have bound states, which can be written as

$$|\psi_b) = \begin{cases} A(\sin \kappa_b r)/(r \sin \kappa_b a), & r < a, \\ A \sinh k_b(R-r)/r \sinh k_b(R-a), & r > a, \end{cases} \tag{A14}$$

where we must have

$$-k_b^2 = \epsilon_b, \quad \kappa_b^2 = V_0 - k_b^2. \tag{A15}$$

The boundary condition at $r=a$ now gives

$$\kappa_b \cot(\kappa_b a) = -k_b \coth k_b(R-a), \tag{A16}$$

which can again be solved with the Newton-Raphson method. The number of bound states, n_b, supported by the potential, is determined by V_0. If

$$n\pi < a V_0^{1/2} < (2n+1)\pi/2, \tag{A17}$$

we have $n_b = n$. If

$$(2n-1)\pi/2 < a V_0^{1/2} < n\pi, \tag{A18}$$

we must distinguish between two cases. If $\tan(aV_0^{1/2}) > -V_0^{1/2}(R-a)$, we have $n_b = n$, whereas $n_b = n-1$ if $\tan(aV_0^{1/2}) < -V_0^{1/2}(R-a)$.

3. Attractive δ shell

In this case the continuum wave functions can be written as

$$|\psi_m) = \begin{cases} A(\sin k_m r)/(r \sin k_m a), & r < a, \\ A[\sin k_m(R-r)]/[r \sin k_m(R-a)], & r > a. \end{cases} \tag{A19}$$

Here A is again a normalization constant, and the wave function must satisfy the boundary condition at $r=a$

$$k_m \sin(k_m R) = V_0 a \sin(k_m a)\sin[k_m(R-a)]. \tag{A20}$$

If a and $V_0 a$ are known, Eq. (A19) can be used to calculate the allowed wave vectors k_m.

For the case of the δ shell we specify the strength $V_0 a$ of the potential, after which the radius a can be determined from δ_0. Before determining this radius, we obtain the perturbed Fermi wave vector, by writing the wave function with energy equal to the perturbed Fermi energy as

$$|\psi_F) = \begin{cases} A(\sin k_F' r)/(r \sin k_F' a), & r < a, \\ A[\sin(k_F' r + \delta_0)]/[r \sin(k_F' a + \delta_0)], & r > a. \end{cases} \tag{A21}$$

From the boundary condition at $r=R$ we obtain

$$k_F' = (N\pi - \delta_0)/R = k_F^0 - \delta_0/R. \tag{A22}$$

The wave functions given in Eq. (A21) must satisfy the boundary condition at $r=a$:

$$\cos(2k_F' a + \delta_0) = \cos(\delta_0) - (2k_F'/V_0 a)\sin(\delta_0), \tag{A23}$$

which can be solved for a. This equation does not determine a uniquely, however, and therefore we always require a to satisfy

$$0 < 2k_F' a + \delta_0 < \pi. \tag{A24}$$

The attractive δ shell can produce a bound state if the potential is strong enough. The bound-state wave function can be written as

$$|\psi_b) = \begin{cases} A(\sinh k_b r)/(r \sinh k_b a), & r < a, \\ A[\sinh k_b(R-r)]/[r \sinh k_b(R-a)], & r > A, \end{cases} \quad \text{(A25)}$$

with boundary condition at $r=a$ given by

$$k_b \sinh(k_b R) = V_0 a \sinh(k_b a)\sinh[k_b(R-a)]. \quad \text{(A26)}$$

This equation has one, and only one, solution if

$$V_0 a^2(1-a/R) > 1. \quad \text{(A27)}$$

The wave vector k_b for this solution can be obtained from Eq. (A26).

4. Repulsive δ shell

The wave functions for this case are again given by Eq. (A19), but now with boundary condition

$$k_m \sin(k_m R) = -V_0 a \sin(k_m a)\sin[k_m(R-a)]. \quad \text{(A28)}$$

For the wave function with energy equal to the perturbed Fermi energy we write

$$|\psi_F) = \begin{cases} A(\sin k_F' r)/(r \sin k_F a), & r < a, \\ A[\sin(k_F' r - \delta_0)]/[r \sin(k_F' a - \delta_0)], & r > a, \end{cases} \quad \text{(A29)}$$

and we obtain for the perturbed Fermi wave vector k_F' in the same way as for the attractive δ shell

$$k_F' = k_F^0 + \delta_0 R, \quad \text{(A30)}$$

after which the radius a of the potential can be determined from the boundary condition at $r=a$,

$$\cos(2k_F' a - \delta_0) = \cos(\delta_0) - (2k_F'/V_0 a)\sin(\delta_0), \quad \text{(A31)}$$

and to determine a uniquely, we require

$$0 < 2k_F' a - \delta_0 < \pi. \quad \text{(A32)}$$

*Present address: Applied Physics Division, California Institute of Technology, Pasadena, California 91125.

[1] H. W. B. Skinner, Philos. Trans. R. Soc. London, Ser. A **239**, 95 (1940).

[2] D. H. Tomboulian, in *The Experimental Method of Soft X-Ray Spectroscopy and the Valence Band Spectra of the Light Elements*, edited by S. Flügge, Handbüch Der Physik Vol. 30 (Springer, Berlin, 1957), p. 246.

[3] R. S. Crisp and S. E. Williams, Philos. Mag. **6**, 365 (1961).

[4] J. A. Catterall and J. Trotter, Philos. Mag. **7**, 671 (1962).

[5] R. Haensel, G. Keitel, P. Schreiber, B. Sonntag, and C. Kunz, Phys. Rev. Lett. **23**, 528 (1969).

[6] R. Haensel, G. Keitel, B. Sonntag, C. Kunz, and P. Schreiber, Phys. Status Solidi A **2**, 85 (1970).

[7] C. Kunz, R. Haensel, G. Keitel, P. Schreiber, and B. Sonntag, in *Electronic Density of States*, Nat. Bur. Stand. (U.S.) Spec. Publ. No. 323, edited by L. H. Bennett (U.S. GPO, Washington, D.C., 1971), p. 275.

[8] T. A. Callcott, E. T. Arakawa, and D. L. Ederer, Phys. Rev. B **18**, 6622 (1978); Jpn. J. Appl. Phys., Suppl. **17** (2), 149 (1978).

[9] S. Sato, T. Miyahara, T. Hanyu, S. Yamaguchi, and T. Ishii, J. Phys. Soc. Jpn. **47**, 836 (1979).

[10] S. C. Slusky, S. E. Schnatterly, and P. C. Gibbons, Phys. Rev. B **20**, 379 (1979).

[11] K. Saito and T. Sagawa, in Proceedings of the Sixth International Conference on Vacuum Ultraviolet Radiation Physics, edited by R. C. Elton, 1980 (unpublished), p. I-78.

[12] K. das Gupta and E. Wood, Philos. Mag. **46**, 77 (1955).

[13] J. A. Catterall and J. Trotter, Philos. Mag. **4**, 1164 (1959).

[14] R. S. Crisp and S. E. Williams, Philos. Mag. **5**, 1205 (1960).

[15] A. Appleton and C. Curry, Philos. Mag. **12**, 245 (1965).

[16] C. Senemaud and C. Hague, J. Phys. (Paris), Colloq. **32**, C4-193 (1971).

[17] H. Neddermeyer, in *Band Structure Spectroscopy of Metals and Alloys*, edited by D. J. Fabian and L. M. Watson (Academic, London, 1973), p. 153.

[18] S. G. Slusky, P. C. Gibbons, S. E. Schnatterly, and J. R. Fields, Phys. Rev. Lett. **36**, 326 (1976).

[19] R. S. Crisp, J. Phys. F: Met. Phys. **10**, 511 (1980).

[20] R. S. Crisp, in *Inner Shell and X-Ray Physics of Atoms and Solids*, edited by D. J. Fabian, H. Kleinpoppen, and L. M. Watson (Plenum, New York, 1981), pp. 625 and 837.

[21] G. A. Rooke, J. Phys. C **1**, 767 (1968); **1**, 776 (1968).

[22] H. Neddermeyer, Phys. Lett. **44A**, 181 (1973).

[23] O. Aita and T. Sagawa, J. Phys. Soc. Jpn. **27**, 164 (1969).

[24] P. Norris, Phys. Lett. **45A**, 387 (1973).

[25] T. Ishii, Y. Sakisaka, S. Yamaguchi, R. Hanyu, and H. Ishii, J. Phys. Soc. Jpn. **42**, 876 (1977).

[26] T. Miyahara, S. Sato, T. Hanyu, A. Kakizaki, S. Yamaguchi, and T. Ishii, in Proceedings of the Sixth International Conference on Vacuum Ultraviolet Radiation Physics (Ref. 11), p. I-73.

[27] A. K. Sen, Indian J. Phys. **30**, 415 (1956).

[28] D. E. Bedo and D. H. Tomboulian, Phys. Rev. **109**, 35 (1958).

[29] J. A. Catterall and J. Trotter, Philos. Mag. **3**, 1423 (1958).

[30] B. F. Sonntag, J. Phys. F: Met. Phys. **3**, L255 (1974).

[31] C. Kunz, H. Petersen, and D. W. Lynch, Phys. Rev. Lett. **33**, 1556 (1974); for a different viewpoint by one of these authors, see H. Petersen, *ibid.* **35**, 1363 (1975).

[32] N. Kosuch, G. Wiech, and A. Faessler, in *Proceedings of the Fourth International Conference on Vacuum Radiation Physics*, edited by E. E. Koch, R. Haensel, and C. Kunz (Pergamon/Vieweg, Braunschweig, 1974), p. 663.

[33] J. Ritsko, S. Schnatterly, and P. Gibbons, Phys. Rev. B **10**, 5017 (1974).

[34] R. S. Crisp, Philos. Mag. **36**, 609 (1977).

[35] T. A. Callcott, E. T. Arakawa, and D. L. Ederer, Phys. Rev. B **16**, 5185 (1977).

[36] T. A. Callcott and E. T. Arakawa, Phys. Rev. Lett. **38**, 442 (1977).

[37] B. Gale, J. A. Catterall, and J. Trotter, Philos. Mag. **20**, 79 (1969).

[38] J. H. Slowik and F. C. Brown, Phys. Rev. Lett. **29**, 934 (1972); J.

H. Slowik, Phys. Rev. B **10**, 416 (1974).
[39] D. J. Phelps, R. A. Tilton, and C. P. Flynn, Phys. Rev. B **14**, 5254 (1976).
[40] B. Gale, Proc. Phys. Soc. London **84**, 933 (1964).
[41] J. A. Tagle, E. T. Arakawa, and T. A. Callcott, Phys. Rev. B **22**, 2716 (1980).
[42] For a review of earlier work and references to the literature, see J. D. Dow, Comments Solid State Phys. **6**, 71 (1975).
[43] J. Friedel, Philos. Mag. **43**, 153 (1952).
[44] J. Friedel, Philos. Mag. **43**, 1115 (1952).
[45] G. D. Mahan, Phys. Rev. **163**, 612 (1967); Solid State Phys. **29**, 75 (1974).
[46] Y. Mizuno and K. Ishikawa, J. Phys. Soc. Jpn. **25**, 627 (1968).
[47] P. Nozières and C. T. De Dominicis, Phys. Rev. **178**, 1097 (1969); B. Roulet, J. Gavoret, and P. Nozières, *ibid.* **178**, 1072 (1968); P. Nozières, J. Gavoret, and B. Roulet, *ibid.* **178**, 1084 (1969).
[48] J. Friedel, Comments Solid State Phys. **2**, 21 (1969).
[49] J. J. Hopfield, Comments Solid State Phys. **2**, 40 (1969).
[50] A. W. Overhauser, quoted by A. J. McAlister, Phys. Rev. **186**, 595 (1969).
[51] G. Ausman, Jr. and A. J. Glick, Phys. Rev. **183**, 687 (1969); Phys. Rev. B **1**, 942 (1970).
[52] S. Doniach and M. Sunjic, J. Phys. C **3**, 285 (1970).
[53] M. Combescot and P. Nozières, J. Phys. (Paris) **32**, 913 (1971).
[54] J. D. Dow, J. E. Robinson, and T. R. Carver, Phys. Rev. Lett. **31**, 759 (1973).
[55] J. D. Dow and D. L. Smith, J. Phys. F: Met. Phys. **3**, L170 (1973).
[56] J. D. Dow, Phys. Rev. Lett. **31**, 1132 (1973).
[57] J. D. Dow and B. F. Sonntag, Phys. Rev. Lett. **31**, 1461 (1973).
[58] J. D. Dow, J. E. Robinson, J. H. Slowik, and B. F. Sonntag, Phys. Rev. B **10**, 432 (1974).
[59] D. R. Franceschetti and J. D. Dow, J. Phys. F: Met. Phys. **4**, L151 (1974).
[60] J. D. Dow, in *Proceedings of the Fourth International Conference on Vacuum Ultraviolet Radiation Physics* (Ref. 32), p. 649.
[61] A. Kotani and Y. Toyozawa, J. Phys. Soc. Jpn. **37**, 912 (1974).
[62] J. D. Dow, in Proceedings of the 12th International Conference on the Physics of Semiconductors, Stuttgart, 1974, pp. 957–961; see also R. J. Elliott, Phys. Rev. **108**, 1384 (1957).
[63] J. D. Dow, L. N. Watson, and D. J. Fabian, J. Phys. F: Met. Phys. **4**, L76 (1974).
[64] J. D. Dow and D. R. Franceschetti, Phys. Lett. **50A**, 1 (1974).
[65] S. Doniach and E. H. Sondheimer, *Green's Functions for Solid State Physicists* (W. A. Benjamin, Reading, MA, 1974).
[66] D. L. Smith and J. D. Dow, Phys. Rev. B **9**, 2509 (1974).
[67] J. D. Dow, Phys. Rev. B **9**, 4165 (1974).
[68] J. D. Dow, J. E. Robinson, J. H. Slowik, and B. F. Sonntag, Phys. Rev. B **10**, 432 (1974).
[69] J. D. Dow, D. L. Smith, and B. F. Sonntag, Phys. Rev. B **10**, 3092 (1974).
[70] J. D. Dow, Phys. Fenn. **9**, Suppl. S1, 341 (1974).
[71] J. D. Dow and D. L. Smith, Phys. Status Solidi B **63**, 635 (1974).
[72] C. P. Flynn, Phys. Rev. Lett. **37**, 1445 (1976).
[73] J. D. Dow and D. R. Franceschetti, Phys. Rev. Lett. **34**, 1320 (1975).
[74] J. D. Dow, D. R. Franceshetti, P. C. Gibbons, and S. E. Schnatterly, J. Phys. F: Met. Phys. **5**, L211 (1975).
[75] J. D. Dow, J. Phys. F: Met. Phys. **5**, 1113 (1975).
[76] Y. Onodera, J. Phys. Soc. Jpn. **39**, 1482 (1975).
[77] J. D. Dow, Comments Solid State Phys. **6**, 71 (1975).
[78] J. D. Dow, D. R. Franceschetti, and D. L. Smith, Phys. Rev. B **11**, 684 (1975).
[79] J. E. Robinson and J. D. Dow, Phys. Rev. B **11**, 5203 (1975).
[80] R. P. Gupta and A. J. Freeman, Phys. Lett. **59A**, 223 (1976).
[81] R. P. Gupta and A. J. Freeman, Phys. Rev. Lett. **36**, 1194 (1976).
[82] R. P. Gupta, A. J. Freeman, and J. D. Dow, Phys. Lett. **59A**, 226 (1976).
[83] J. D. Dow and John E. Robinson, Phys. Rev. B **14**, 2683 (1976).
[84] C. P. Flynn, Phys. Rev. B **14**, 5294 (1976).
[85] C. O. Almbladh and U. von Barth, Phys. Rev. B **13**, 3307 (1976).
[86] P. Minnhagen, Phys. Lett. **56A**, 327 (1976); for an explanation of why this author finds such surprising results in the special case he has considered, see Ref. 87.
[87] Y. Ohmura, in *Inner Shell and X-Ray Physics of Atoms and Solids* (Ref. 20), p. 555; Y. Ohmura and K. Ishikawa, J. Phys. Soc. Jpn. **48**, 1176 (1980), and references therein.
[88] J. D. Dow, Philos. Mag. **35**, 837 (1977).
[89] J. D. Dow, D. L. Smith, D. R. Franceschetti, J. E. Robinson, and T. R. Carver, Phys. Rev. B **16**, 4707 (1977).
[90] J. D. Dow and C. P. Flynn, J. Phys. C **13**, 1341 (1980); this work was summarized in J. D. Dow, Nuovo Cimento Soc. Ital. Fis., B **39**, 465 (1977).
[91] N. D. Lang and A. R. Williams, Phys. Rev. B **16**, 2408 (1977).
[92] V. I. Grebbenikov, Yu. A. Babanov, and O. B. Sokolov, Phys. Status Solidi B **79**, 423 (1977); **80**, 73 (1977); V. I. Grebbinikov, O. B. Sokolov, and E. A. Turov, *ibid.* **84**, 773 (1977); **85**, 127 (1978); O. B. Sokolov, V. I. Grebbinikov, and E. A. Turov, Fiz. Met. Metalloved. **43**, 1311 (1977); Phys. Status Solidi B **83**, 281 (1977); Yu. A. Matveev, V. I. Grebbinikov, and O. B. Sokolov, Fiz. Met. Metalloved. **48**, 80 (1979).
[93] K. Schönhammer and O. Gunnarson, Solid State Commun. **26**, 399 (1978); Phys. Rev. B **18**, 6606 (1978).
[94] M. A. Kolber and J. D. Dow, J. Phys. Soc. Jpn. **45**, 855 (1978).
[95] J. D. Dow and C. P. Flynn, J. Phys. C **13**, 1341 (1980).
[96] C. A. Swarts, J. D. Dow, and C. P. Flynn, Phys. Rev. Lett. **43**, 158 (1979).
[97] L. C. Davis and L. A. Feldkamp, J. Appl. Phys. **50**, 1944 (1979).
[98] W. Domcke, L. S. Cederbaum, J. Schirmer, and W. von Niessen, Phys. Rev. Lett. **42**, 1237 (1979).
[99] M. A. Bowen and J. D. Dow, Semicond. Insul. **5**, 85 (1980).
[100] M. A. Bowen and J. D. Dow, Phys. Rev. B **22**, 220 (1980).
[101] M. A. Bowen and J. D. Dow, Phys. Rev. B **23**, 671 (1981).
[102] P. A. Cox, in *Inner Shell and X-Ray Physics of Atoms and Solids* (Ref. 20), p. 549.
[103] P. Longe, in *Inner Shell and X-Ray Physics of Atoms and Solids* (Ref. 20), p. 533; S. M. Bose, P. Kiehn, and P. Longe, in *ibid.* p. 489. These papers summarize the extensive contributions of Longe and co-workers.
[104] W. Hänsch and W. Eckhardt, in *Inner Shell and X-Ray Physics of Atoms and Solids* (Ref. 20), p. 563.
[105] R. C. Desjonqueres, D. Spanjaard, Y. Lassailly, and C. Guillot, in Proceedings of the Sixth International Conference on Vacuum Ultraviolet Radiation Physics (Ref. 11), p. I-27; G. Treglia, F. Ducastelle, M. C. Desjonqueres, and D. Spanjaard, in *ibid.* p. I-39; G. Treglia, F. Ducastelle, and D. Spanjaard, J. Phys. (Paris) **41**, 281 (1980).
[106] J. D. Dow, E. Mehreteab, and C. A. Swarts, Philos. Mag. B **45**, 519 (1982).

[107] M. A. Bowen and J. D. Dow, Int. J. Mod. Phys. B **2**, 1483 (1988); see also A. Yoshimori and A. Okiji, Phys. Rev. B **16**, 3838 (1977); S. Girvin and J. J. Hopfield, Phys. Rev. Lett. **37**, 1091 (1976).

[108] L. A. Feldkamp and L. C. Davis, Phys. Rev. B **22**, 4994 (1980).

[109] The possibility that incomplete lattice relaxation [C. O. Almbladh, Phys. Rev. B **16**, 4343 (1977); see also C. O. Almbladh and P. Minnhagen, Phys. Status Solidi B **85**, 135 (1978)] is responsible for one feature in the *K* edge of Li (Ref. 35) may be ruled out by the recent experiments of Crisp (Ref. 20), which showed absorption and emission edges overlapping, even when the incomplete relaxation knee disappears.

[110] The Thomas-Fermi potentials had bound states, an artifact of the Thomas-Fermi approximation. There has been a recent attempt [U. von Barth and G. Grossman, Solid State Commun. **32**, 645 (1979)] to reestablish the original theory with these large phase shifts; this attempt has established contact with analyses of XPS data which purport to find large phase shifts (Ref. 24), in conflict with a large body of data, most notably impurity resistivity (Ref. 74) and electron energy loss (Refs. 33, 83, and 88).

[111] C. Noguera, D. Spanjaard, and J. Friedel, J. Phys. F: Met. Phys. **9**, 1189 (1979); C. Noguera and D. Spanjaard, *ibid.* **11**, 1133 (1981).

[112] J. N. Schulman and J. D. Dow, Phys. Rev. Lett. **47**, 1133 (1981).

[113] M. A. Bowen and J. D. Dow, Nuovo Cimento Soc. Ital. Fis., D **1**, 587 (1982).

[114] J. D. Dow, C. A. Swarts, M. A. Bowen, E. Mehreteab, and S. S. Satpathy, in *Inner Shell and X-Ray Physics of Atoms and Solids* (Ref. 20), p. 559.

[115] E. Müller-Hartmann, T. V. Ramakrishnan, and G. Toulouse, Phys. Rev. B **3**, 1102 (1971).

[116] K. Ohtaka and Y. Tabnabe, Phys. Rev. B **28**, 6833 (1983); **30**, 4235 (1984).

[117] M. S. Skolnick, J. M. Rorison, K. Nash, D. J. Mowbray, P. R. Tapster, S. J. Bass, and A. D. Pitt, Phys. Rev. Lett. **58**, 2130 (1987).

[118] R. Sooryakumar, A. Pinczuk, A. C. Gossard, D. S. Chemla, and L. J. Sham, Phys. Rev. Lett. **58**, 1150 (1987).

[119] M. Potemski, R. Stepniewski, J. C. Maan, G. Martinez, P. Wyder, and B. Etienne, Phys. Rev. Lett. **66**, 2239 (1991).

[120] K. J. Nash, M. S. Skolnick, M. K. Saker, and S. J. Bass, Phys. Rev. Lett. **70**, 3115 (1993).

[121] I. Hapke-Wurst, U. Zeitler, H. Frahm, A. G. M. Jansen, R. J. Haug, and K. Pierz, Phys. Rev. B **62**, 12621 (2000).

[122] T. Schauerte, J. Kroha, and P. Wölfle, Phys. Rev. B **62**, 4394 (2000).

[123] E. Bascones, C. P. Herrero, F. Guinea, and G. Schön, Phys. Rev. B **61**, 16778 (2000).

[124] T. Privalov, F. Gel'mukhanov, and H. Ågren, Phys. Rev. B **64**, 165115 (2001).

[125] K. Kaule, S. Krichner, J. Kroha, and P. Wölfle, Phys. Rev. B **64**, 155111 (2001).

[126] S. Tanaka, V. Chernyak, and S. Mukamel, Phys. Rev. A **63**, 063405 (2001).

[127] D. Porras, J. Fernandez-Rossier, and C. Tejedor, Phys. Rev. B **63**, 245321 (2001).

[128] S. Nomura, T. Nakanishi, and Y. Aoyagi, Phys. Rev. B **63**, 165330 (2001).

[129] M. N. R. Wohlfarth and L. S. Cederbaum, Phys. Rev. A **65**, 052703 (2002).

[130] T. Melin and F. Laruelle, Phys. Rev. Lett. **85**, 852 (2000); Phys. Rev. B **65**, 195303 (2002).

[131] L. Ley, F. R. McFeely, S. P. Kowalczyk, J. G. Jenkin, and D. A. Shirley, Phys. Rev. B **11**, 600 (1975).

[132] G. K. Wertheim and S. Hüfner, Phys. Rev. Lett. **35**, 53 (1975); S. Hüfner and G. K. Wertheim, Phys. Rev. B **11**, 678 (1975).

[133] P. H. Citrin, G. K. Wertheim, and Y. Baer, Phys. Rev. Lett. **35**, 885 (1975).

[134] Y. Baer, P. H. Citrin, and G. K. Wertheim, Phys. Rev. Lett. **37**, 49 (1976).

[135] P. H. Citrin, G. K. Wertheim, and M. Schlüter, Phys. Rev. B **20**, 3067 (1979).

[136] Strictly speaking, the infinite repulsive barrier potential we use does not satisfy the sum rules, because the wave functions in the presence of the barrier are zero and do not form a complete set within the barrier. This problem is circumvented by considering the limit of large but finite barrier heights (Ref. 113).

[137] The exponents are $\alpha_\ell = (2\delta_\ell/\pi) - \Sigma_{j=0} 2(2j+1)(\delta_j/\pi)^2$.

[138] S. Satpathy and J. D. Dow, J. Phys. Chem. Solids **47**, 109 (1986).

[139] S. Satpathy and J. D. Dow, Solid State Commun. **42**, 637 (1982).

[140] S. Satpathy and J. D. Dow, Phys. Rev. B **25**, 6083 (1982).

[141] S. Satpathy, J. D. Dow, and M. A. Bowen, Phys. Rev. B **28**, 4255 (1983).

[142] L. N. Oliveira, Ph.D. thesis, Cornell University, 1981.

[143] P. W. Anderson, Phys. Rev. Lett. **18**, 1049 (1967); Phys. Rev. **164**, 352 (1967).

[144] C. A. Swarts and J. D. Dow (unpublished).

[145] This expression is obtained if one uses free-electron wave functions.

[146] To find the zero of $f(x)$, form the successive approximations $x_{n+1} = x_n - f(x_n)/f'(x_n)$.